Journal of the mechanical behavior of biomedical materials 73 (2017) 50–67

Contents lists available at ScienceDirect

Journal of the Mechanical Behavior of Biomedical Materials

journal homepage: www.elsevier.com/locate/jmbbm

The turtle carapace as an optimized multi-scale biological composite armor – A review

Ben Achrai, H. Daniel Wagner*

Department of Materials & Interfaces, Weizmann Institute of Science, Rehovot 76100, Israel

ARTICLE INFO

Keywords:
Turtle shell
Biological composites
Hierarchical structure
Bio-inspired materials
Mechanical properties
Functionally graded materials

ABSTRACT

The turtle carapace, the top dorsal part of the shell, is a remarkable multi-scale dermal armor that has evolved to withstand various types of high-stress events encountered in nature. This keratin-covered boney exoskeleton exhibits a number of structural motifs, including alternating rigid and flexible components, layering and functionally graded elements, designed to protect the reptile during predatory attacks, and smashing events. Here we review the multi-scale structural hierarchy of the turtle carapace and its corresponding mechanical properties. We show how the microscopic features of the carapace govern its various macroscopic mechanical responses relevant to protective functioning, including dynamic (impact and cyclic) compression and bending loading situations. In addition, the effect of hydration, a crucial factor for proper physiological-mechanical behavior of biological materials, is illustrated throughout. We also discuss carapace-inspired designs that could be advantageous over the traditional strategies adopted in impact-resistant materials, and could bring new mechanistic insights.

1. Introduction

The turtle shell is an exceptional biological structure that, for centuries, has fascinated researchers from a wide range of disciplines, including evolutionary and developmental biology (Gilbert et al., 2001; Lyson et al., 2013), bio-chemistry (Jackson, 2002), bio-physics (Gaunt and Gans, 1969), and materials science and mechanical engineering (Balani et al., 2011; Rhee et al., 2009). Descriptive morphological studies of turtle shells have been published many years ago (e.g., (Bojanus, 1819)), while active research is still being conducted (Lyson et al., 2016; Scheyer and Sánchez-Villagra, 2007; Scheyer et al., 2014; Scheyer et al., 2015). However, it is only in the last decade, as part of the increasing interest in biological and bio-inspired materials research (Bar-On et al., 2014; Chintapalli et al., 2014; Naleway et al., 2016; Zhu et al., 2013) and specifically in biological impact-resistant armors (Ehrlich, 2015; Li and Ortiz, 2014; Sun and Chen, 2013; Torres et al., 2015; Zimmermann et al., 2013), that the structural-mechanical properties of the turtle shell have gained considerable attention (Achrai and Wagner, 2013, 2015; Achrai et al., 2014, 2015; Balani et al., 2011; Damiens et al., 2012; Magwene and Socha, 2013; Rhee et al., 2009; Krauss et al., 2009). This is mainly due to (i) massive advances in experimental techniques, computer-aided modeling and theoretical foundations; (ii) global convergence into a multidisciplinary bio-materials research involving biology, chemistry, physics, engineering and mathematics; (iii) a drive to develop novel materials for various applications. In particular, innovative impact-resistant light-weight structures that exhibit properties that are usually mutually exclusive - such as high specific stiffness and toughness - are mostly sought-after.

Turtles (including tortoises, hard-shelled, soft-shelled and leatherback species) belong to the order Testudines of the class Reptilia and are considered to have existed since the Triassic era, dating back to ~200 million years ago (Gilbert et al., 2001). Turtles possess a keratin-covered dome-shaped multi-functional dermal shell. The shell consists of the dorsal carapace and the ventral plastron (Fig. 1a), which are connected by lateral bridges between the front and hind limbs. The carapace exhibits multi-scale compositional-structural complexity that translates into unique biophysical functionalities such as camouflage, waterproofing (Alibardi and Toni, 2006), buoyancy (Krauss et al., 2009), reservoir for metabolites (e.g., fat and ions) (Balani et al., 2011), and predominantly, for mechanical protection.

With regard to its defensive role, although currently under debate (Lyson et al., 2016), the shell is believed to have evolved to protect the reptile against extreme mechanical forces encountered during predator attacks. The latter include sharp high strain-rate assaults exerted by, among others, alligators (Erickson et al., 2003), jaguars (Emmons, 1989; Christiansen and Wroe, 2007) sharks (Heithaus et al., 2008) and birds, in the form of biting, clawing or pecking (Magwene and Socha, 2013). Some of these high-stress loads are likely applied in a low-

* Corresponding author.
E-mail addresses: Ben.Achrai@weizmann.ac.il (B. Achrai), Daniel.Wagner@weizmann.ac.il (H.D. Wagner).

http://dx.doi.org/10.1016/j.jmbbm.2017.02.027
Received 15 September 2016; Received in revised form 19 February 2017; Accepted 24 February 2017
Available online 27 February 2017
1751-6161/

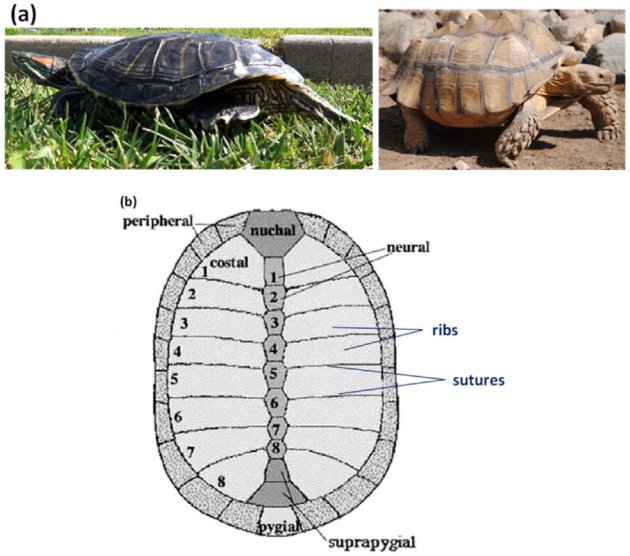

Fig. 1. (a). Left - Red-eared slider turtle (*Trachemys scripta elegans*), showing a fairly flat carapace. Right - African spurred tortoise (*Centrochelys sulcata)*, showing a high-dome and bumpy carapace (b) Predominant pattern of the carapacial bones. The ribs and sutures are indicated. Numbering of the neural and costal bones is shown. Fig (c) was adapted with permission from (Gilbert et al., 2001).

frequency repetitive (cyclic) manner, and involve bending of the shell along with compression and local indentation. Avian predators (e.g., eagles) also use an additional offensive strategy, in which the turtle is dropped from great heights onto rocks and the shell is subjected to blunt impact blows when hitting the ground and eventually fractures (Branch and Els, 1990; Walley, 1993). The shell may also undergo blunt impact loads through falling and smashing against rocks in lotic (streaming) ecosystems and high-tide environments.

In the present review we focus on the multi-scale structure-mechanical function connection of the carapace of hard-shelled turtles, predominantly (unless indicated otherwise) of the red-eared slider turtle (*Trachemys scripta elegans*) due to extensive research conducted on that species. We aim to present in-depth and integrative understanding of how the hierarchically-structured carapace protectively functions under diverse loading conditions, which may arise during natural situations such as predator attacks (e.g., impact and/or high-stress cyclic loads) or crushing against rocks (impact blows). The layout of this review consists of the following: (a) Structural overview; (b) Systematic compositional and micro-structural characterization of the boney and the keratinous regions, along with their local mechanical properties; (c) Assessment of the quasi-static mechanical properties of the carapace sub-regions while taking into account the microscopic features; (d) Evaluation of the carapace behavior under dynamic loading events such as impact and high-stress cyclic flexural loads; (e) Whole shell examination; (f) Resistance of the carapace to penetration loads; (g) Integration of the carapace sub-regions into an efficient whole shield; (g) Bio-inspired aspects and implications for future innovative armor designs.

Since turtles are semi-aquatic species and mostly found inside water reservoirs (lakes, rivers, seas etc.) and their carapace is filled with water (acting as a pH buffer (Gilbert et al., 2001)). The effect of hydration will therefore also be addressed. Furthermore, from the materials science point of view, which set the basis for engineered armor material production and performance, a comparison between the dry and wet properties will be held (when possible).

2. Structural overview of the turtle carapace

The carapace is mainly composed of bone tissues, and as is well known, these exhibit a multi-scale structural hierarchy, starting from the main constituents: type I collagen helices, hydroxyapatite nano-platelets and water (non-collagenous proteins are also present in minor quantities) (Weiner and Wagner, 1998). These form mineralized collagen fibrils - the basic composite building blocks of all bones – which are assembled into micrometer-thick fibers and fiber bundles possessing fibrillar structures such as the parallel-fibered, woven, radial and plywood arrays (Fig. 2a). Combinations of the previous arrays are common, while the most abundant array is the plywood pattern, which is found in concentric lamellae forming the osteonal unit. At the macro-level, compact (cortical) and foamy (trabecular, cancellous) bones arrange together to form whole bones of various types, adapted to different mechanical purposes (e.g., structural support by the stiff long bones of limbs, vibrational conductance by the brittle auditory bulla (Currey, 2002), combat weapons by the tough deer antler (Launey et al, 2009)).

The boney carapace (along with the plastron) is coated by an epidermal keratinous layer, usually divided into 38 scutes, arranged in a mosaic-like pattern, which are not in registry with the underneath bones (Gilbert et al., 2001) (Fig. 2h-i). The relatively rigid and hard outer layer (stratum corneum) is composed of mostly β-pleated sheet (and some α-helix (Dalla Valle et al., 2013; Alibardi, 2013)) fibril-reinforced keratin matrix that also embeds dead cornified cells (Alibardi and Thompson, 2006; McKittrick et al., 2012). Underneath, layers consisting of fibril-reinforced keratin matrix embedding keratinocytes, melanocytes, pigments and lipids are present. The keratin coating fulfills several physiological functions such as physico-chemical barrier, heat regulator, reduction of hydrodynamic drag forces and camouflage. It also serves as the first line of defense to resist various low and high strain-rate loading conditions.

The turtle carapace presents a unique macroscopic configuration of alternating stripes of rigid boney ribs attached to each other by compliant collagenous sutures (Gilbert et al., 2001) (Figs. 1b, 2b–f). The ribs are oriented in the medial-lateral (M-L) direction, they emanate from the vertebrae and are fused to dermal (costal, Fig. 1b) bones, eventually terminating at the peripheral bones (Figs. 1b,2a, (Gilbert et al., 2001)). Notably, the vertebrae (neural) and the peripheral bones (~5–10 mm thick) are thicker than the ribs (~3 mm thick), providing the carapace main frame, to which the ribs are attached (Figs. 1b,2a). At the micro-level, the ribs possess a flat-bone sandwich structure in which a cancellous interior is enclosed by dorsal and ventral cortices (Fig. 2b–d). This configuration enables energy absorption (acting as a cushion) and weight reduction, leading to better specific mechanical properties (i.e., stiffness, strength and toughness, (Ashby, 1983)). The porous interior is partially filled with body fluids and thus (i) serves as a metabolic reservoir and as a pH buffer (Gilbert et al., 2001), and (ii) enables buoyancy (Krauss et al., 2009). The ribs are connected to one another by soft unmineralized collagenous fibers spanning the 3D zigzag interlocking sutures (Fig. 2d–f). In addition, these fibers spread laterally from one suture to a neighboring one (Fig. 2f–g), forming the dermis layer which attaches the keratin scutes to the underneath dorsal bone via anchoring fibrils running perpendicularly into the adjacent layers.

3. Microscopic compositional-structural-mechanical properties

In the following the microscopic compositional-structural-mechanical features of the carapace sub-regions are described in detail, beginning with the ribs.

3.1. Ribs

The ribs possess a flat-bone sandwich-like layered structure of two dense dorsal and ventral cortices (each is 0.25–0.75 mm thick) enclosing a cancellous foamy interior (1–3 mm thick, Figs. 2d,3a). The sandwich motif is abundantly found across vertebrate including in skulls (Mao et al., 2011; Motherway et al., 2009), carapaces (of e.g. armadillos (Chen et al.,

2011; Rhee et al., 2011) and turtles (Achrai and Wagner, 2013; Rhee et al., 2009)) and osteoderms (of e.g. alligators (Sun and Chen, 2013)) as well as in synthetic low-weight supporting structures required for applications such as transportation and aviation (Bitzer, 2012). This configuration enables (i) buoyancy, (ii) impact energy absorbance achieved by the foamy interior acting as a cushion (Ashby, 1983) and (iii) weight reduction leading to optimized stiffness-, strength- and toughness-to-weight properties. In Section 4 we show how the cancellous interior contributes to the compression and flexure behaviors of whole ribs.

In addition, the relative density (i.e., the bone volume divided by the tissue volume, ρ) within the ribs of the red-eared slider turtles gradually decreases when approaching from the densely-packed dorsal cortex (ρ≈0.9–0.95) toward the cancellous interior (ρ ≈ 0.4–0.5) (Fig. 3a, (Achrai and Wagner, 2013; Krauss et al., 2009)). Such geometrical gradation induces (i) graded stiffness that is thought to reduce the stiffness mismatch at the dorsal cortex-foamy interior interface and (ii) better interfacial adhesion between the dorsal cortex and the core (foamy interior). These are thought to hamper several modes of failures such as interfacial delamination, and buckling (wrinkling) in the exterior layer and/or the core (intra-cell dimpling) (Petras and Sutcliffe, 1999). Therefore, the rib may be viewed as a functionally graded material (FGM), a key feature that is currently sought after in man-made structures. For example in titanium-based orthopedic implants a graded porosity is used to induce graded stiffness required to prevent stress shielding and promote proper bone remodeling (Thieme et al., 2001).

3.1.1. Cortices

The dorsal and ventral cortex layers feature similar mineral content (~60 wt%, (Achrai and Wagner, 2013)) and relative density; however, they differ markedly in their fibrillar packing arrays and the corresponding mechanical properties. The dorsal cortex exhibits randomly-oriented (boney) fiber bundles surrounding a disordered osteonal network (Fig. 3b-c). The disorganized fibrillar pattern gives rise to isotropic local mechanical properties, i.e. stiffness (E_{dry} ≈ 16.5 GPa, Table 1) and hardness (H_{dry} ≈ 0.65 GPa), which have been shown the be similar in all three anatomical directions (D-V, M-L and A-P, see Fig. 2) (Achrai et al., 2014).

The ventral cortex, on the other hand, possesses a cross-ply (0°/90°) structure with two orthogonal parallel-fibered sub-layers wherein the fibers in the upper and lower layers are oriented with the M-L and A-P axes, respectively (Fig. 3d-f). Nanoindentation measurements show that each sub-layer of the ventral cortex exhibits a transversely isotropic response to load ($E_{\parallel,dry}$ ≈ 18 GPa, $E_{\perp,dry}$ ≈ 12 GPa, Table 1). The anisotropy ratio was found to be comparable with data reported for other parallel-fibered boney tissues (Fratzl et al., 2004; Rho et al., 2001a, 2001b). Furthermore, as expected, hydration was shown to decrease the stiffness and hardness, mainly due to the plasticizing effect of the water molecules, which infiltrate into voids present within peptides, fibrils, fibers, fiber bundles and the extracellular matrix (Guidoni et al., 2009). Through hydrogen bonding interactions with the collagen triple helices, the water molecules induce conformational changes causing swelling and softening of the tissues. Specifically, under physiological (wet) conditions the mechanical anisotropy ratio actually increased by 60% (Table 1), likely due to a higher degree of fibril alignment induced by weakening of lateral peptide–peptide interactions between neighboring chains (Lazarev et al., 1985, 1992).

Nanoindentation measurements performed on cortices of rib specimens taken from the carapaces of the box turtle (*Terrapene carolina,* which possesses a relatively high dome) and the freshwater snapping turtle (*Chelydra serpentina*) yielded elastic moduli in the range of 18–24 GPa and ~22 GPa, respectively (Table 1). In both studies higher stiffness values were obtained in comparison to the red-eared slider turtle carapace (Table 1). This is likely due to the shallower indents observed in those studies, which usually result in higher stiffness (and hardness) values, corresponding to the indentation size effect (ISE). The latter describes monotonic decrease in mechanical properties with increasing indentation depths (and thus volumes) due to damage accumulation (Faingold et al., 2012; Lawn and Cook, 2012) induced by micro-cracking and defects (e.g., canaliculi) present in inherently-heterogeneous boney structures. In addition, the measurements in those studies were performed only on the transverse sections of dry specimens and without addressing the effect of morphology (fibrillar organization) and composition (mineral content); both substantially govern the stiffness properties of boney materials (Weiner and Wagner, 1998).

3.1.2. Cancellous interior

In contrast to the dense cortices, the highly porous cancellous region exhibits a closed-cell trabecular network with a mean trabeculae thickness of ~0.1 mm (Fig. 3g). The lower mineral content (~50 wt%, (Achrai and Wagner, 2013)) in this region coincides with lower stiffness and hardness values (E_{dry} ≈ 12.5 GPa, H_{dry} ≈ 0.5 GPa) measured by nanoindentation. The lower mineral content (in comparison to the cortices) and higher organic content also result in higher decrease of the mechanical properties when measured under wet conditions. This is because the water molecules form hydrogen bonds that mostly alter the loose structure of the organic molecules (in comparison to the tight crystalline mineral nano-platelets) which in turn reduce the mechanical properties. In addition, the presence of unmineralized fibers spanning trabecular voids (Fig. 3g) (Achrai and Wagner, 2013; Rhee et al., 2009), a characteristic of woven bone (Achrai and Wagner, 2013), are assumed to strengthen the cellular region by stretching and bridging (Balani et al., 2011).

3.2. Suture

Between each two neighboring ribs lies the perisuture, which consists of a compliant unmineralized suture (Figs. 2e,4c,f) possessing a complex 3D interdigitating zigzag architecture where stiff triangular boney tips (from each adjacent rib) are held together by unmineralized collagen fibers (termed Sharpey's fibers, Fig. 4a-b). Perisutures are common in nature and are found in skulls (Jaslow, 1990; Rafferty and Herring, 1999), alligator osteoderms (Sun and Chen, 2013), armadillo carapaces (Chen et al., 2011) and more. They appear with various morphologies (e.g., interdigitated or planar (Chen et al., 2011)) and provide flexibility and toughness to otherwise stiff and brittle elements (e.g., bones (Jaslow, 1990)).

It was shown by histology (Krauss et al., 2009) and fractography (Achrai and Wagner, 2013) that in the red-eared slider turtle carapace the boney fibers composing the tips are roughly oriented along the A-P direction while the unmineralized fibers spanning the suture are oriented at an angle to its sinuous course (Fig. 4a-b). In this morphology the unmineralized fibers are actually loaded in tension along their long axis upon bending of the perisuture, which may occur during low-stress loading activities of the reptile (e.g., locomotion, respiration) and high-stress loading incidents (e.g., predatory attacks, smashing against rocks). This maximizes resistance to deformation (Rafferty and Herring, 1999). Micro-mechanical measurements revealed that the unmineralized collagen fibers are much more compliant (E_{dry} ≈ 1.6 GPa) than the boney tips, especially in the hydrated state which better mimic physiological conditions (E_{wet} ≈ 0.2 GPa). The nanoindentation measurements, performed along the boney see-saw elements, from the boney tip edge towards the boney tips bulk (see indentation trends in Fig. 4c-d) revealed graded stiffness characteristics (E_{wet} ≈ 3.5–7.5 GPa, Fig. 4e). This mechanical trend coincides with the increasing degree of mineralization obtained by segmentation of μCT scanning (Fig. 4f). These graded compositional-mechanical properties provide extra flexibility to the region and additional toughness to the carapace, as will be shown later (see Sections 4.2 and 5). The perisuture region is another example of a functionally graded material, where gradation is achieved by compositional trend (instead of morphological means as was observed in the rib).

Moreover, the boney teeth in the perisuture exhibit a triangular

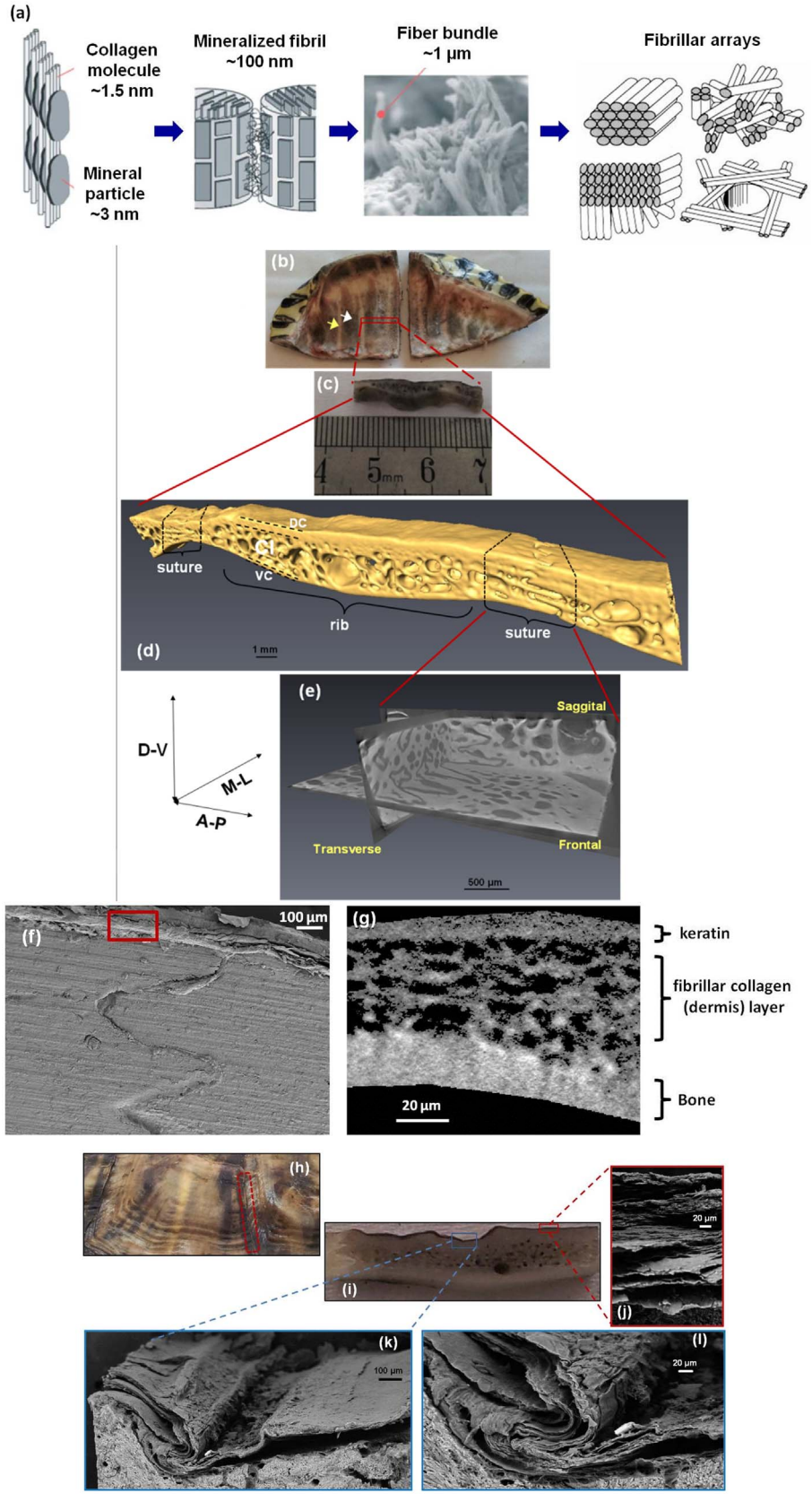
(a)
Collagen molecule ~1.5 nm
Mineral particle ~3 nm
Mineralized fibril ~100 nm
Fiber bundle ~1 μm
Fibrillar arrays
(b)
(c)
(d)
DC
CT
VC
suture
rib
suture
1 mm
D-V
M-L
A-P
(e)
Saggital
Transverse
Frontal
500 μm
(f)
100 μm
(g)
keratin
fibrillar collagen (dermis) layer
Bone
20 μm
(h)
(i)
(j)
20 μm
(k)
100 μm
(l)
20 μm

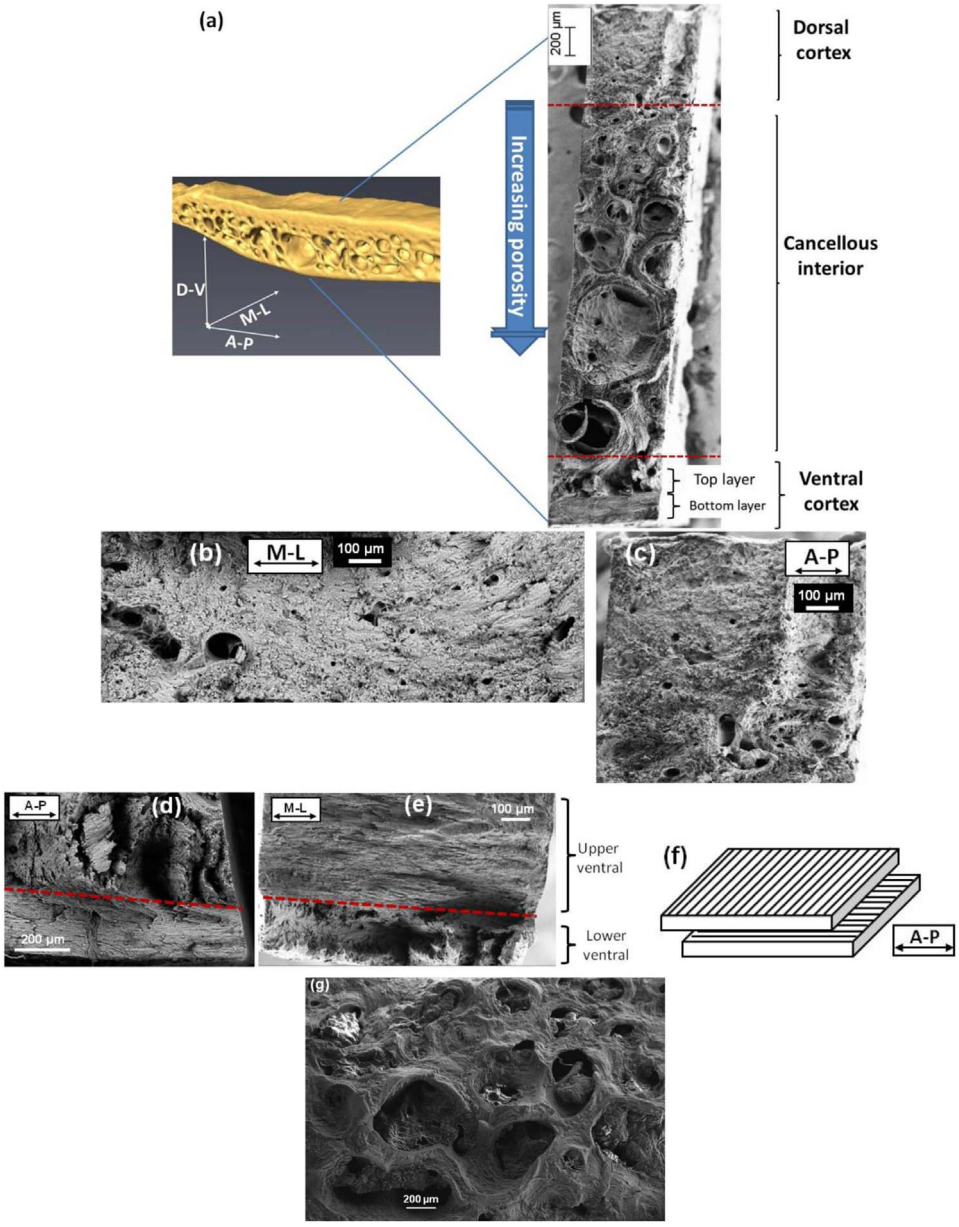

Fig. 3. (a) A µCT reconstruction modified using a SEM fractograph showing the saggital surface of the carapace rib. The fractograph reveals the dorsal and ventral cortices and the cancellous interior of the rib. Increasing porosity is clearly visible when approaching the CI region from the dorsal cortex. (b,c) SEM fractography of the dorsal cortex showing (b) transverse and (c) saggital surfaces. In both fractographs osteons are seen randomly embedded in the woven (disordered) fiber bundle matrix. (d-e) SEM fractography of the ventral cortex showing (d) saggital and (e) transverse surfaces. Two distinct sub-regions are seen (divided by the red dashed line). In (d) the fibers in the lower layer are aligned parallel to the A-P axis, while the fibers in the upper layer are directed perpendicular to the saggital plane. The complementary picture is seen in (e). In the lower layer the fibers appear to be aligned perpendicular to the transverse direction, while the fibers in the upper layer are aligned parallel to the M-L direction. (f) Schematic showing the cross-ply motif of two perpendicular parallel fiber sub-layers found in the VC layer. Figs (a–f) and (g) were adapted with permission from (Achrai and Wagner, 2013) and (Achrai et al., 2014), respectively.

structure with a mean tooth angle θ ≈ 9.4–27.8° (Fig. 4c and (Krauss et al., 2009)). Li et al. (2011) showed by analytical and numerical modeling that a triangular geometry is superior to that of, for instance, a rectangular one in terms of stiffness, strength and stress distribution. These authors developed a model for predicting the strength of a triangular suture possessing a compliant phase (in which E = 0.1 GPa, σ_{max} = 20 MPa) and a stiff phase (in which E = 10 GPa, σ_{max} = 100 MPa), and found that the optimal tooth angle for homogenous stress distribution is 2θ = 23.6°, agreeing well with the morphological observations. However, they assumed a homogenous stiffness and

Fig. 2. (a) Schematic showing the structural hierarchy of bones, which comprise the turtle shell bulk (b) Ventral view of a red-eared slider turtle carapace cut. The white and yellow arrows mark an individual rib and suture, respectively. (c) Section of the rib enclosed by sutures at the edges. (d) Tomographic reconstruction of (c), showing the sandwich arrangement of the rib. The sub-layers forming the rib are indicated as the dorsal cortex (DC), ventral cortex (VC) and the cancellous interior (CI). (e) Ortho-slice view of the suture region (i.e., the perisuture). The unmineralized suture is indicated by the dark curly path. Images (d) and (e) are oriented in the same anatomical position. The anatomical planes (frontal, saggital and transverse) are marked with the anatomical orientations: anterior-posterior (A-P), medial-lateral (M-L) and dorsal-ventral (D-V). (f) Scanning electron microscopy (SEM) image showing cross-section of the perisuture. The unmineralized fibrillar collagenous layer is seen spanning the zigzag suture and emanating laterally, connecting the overlaid keratin scutes to the underling bone. (g) High-resolution micro-computer tomography (µCT) section showing the area marked by the red rectangle in (f). The fibrillar network of the collagen layer is clearly visible, possessing anchoring fiber bundles that run perpendicularly into the adjacent (upper keratin and lower bone) layers. (h) Dorsal surface of a carapace displaying a hinge region (marked by the red dashed rectangle) located between quasi-planar areas of the keratin scutes. (i) Cross-section of the carapace showing planar and folded (hinge) regions. (j–k) SEM fractographs elucidating planar (j) and folded stacking (k,l) of the keratin laminate. Fig (a) was jointly adapted with permission from (Beniash, 2011) and (Weiner and Wagner, 1998). Figs (b–e), (f,g) and (h,l) were adapted with permission from (Achrai et al., 2014), (Achrai et al., 2015) and (Achrai and Wagner, 2013), respectively.

Table 1
Mean elastic modulus (E) and hardness (H) measured by nanoindentation in different regions of carapaces from several turtle species. The reported sub-regions and indentation conditions (hydration state, indenting direction and depth/load) are indicated.[1,2,3] refer to (Achrai and Wagner, 2013), (Rhee et al., 2009) and (Balani et al., 2011), respectively.

Turtle species	Region	Sub-region		Indentation conditions			E (GPa)	H (GPa)
				Hydration state	Direction	Depth/Load		
Red-eared slider (*Trachemys scripta elegans*)[1]	**Keratin scutes**	-		Dry	Perpendicular to laminate	Depth ≈ 2000 nm (deep indents)	3.6 ± 1.5	0.15 ± 0.09
					Frontal plane		4.2 ± 1.1	0.22 ± 0.08
				Wet	Perpendicular to laminate		1.3 ± 0.6	0.04 ± 0.02
					Frontal plane		0.7 ± 0.3	0.02 ± 0.01
	Collagen dermis	(layer includes the unmineralized suture, see Figs. 2,5)		Dry	Frontal and Saggital average		1.6 ± 0.9	0.06 ± 0.05
				Wet	Frontal and Saggital average		0.2 ± 0.08	0.007 ± 0.003
	Rib	Dorsal cortex		Dry	Transverse plane		16.7 ± 2.6	0.67 ± 0.15
					Saggital plane		16.6 ± 2.2	0.63 ± 0.15
					Frontal plane		16.4 ± 2.4	0.63 ± 0.13
				Wet	Spatial average		11.2 ± 1.5	0.28 ± 0.08
		Cancellous interior		Dry	Spatial average		12.6 ± 1.7	0.49 ± 0.11
				Wet	Spatial average		6.7 ± 1.3	0.18 ± 0.07
		Ventral cortex	Top layer	Dry	Transverse plane		12.3 ± 1.8	0.48 ± 0.13
					Saggital plane		18.2 ± 1.8	0.67 ± 0.09
					Frontal plane		11.8 ± 1.5	0.50 ± 0.08
			Bottom layer	Dry	Transverse plane		17.9 ± 2.0	0.62 ± 0.11
					Saggital plane		12.7 ± 1.5	0.45 ± 0.12
					Frontal plane		11.6 ± 1.3	0.43 ± 0.07
			Both layers	Wet	Parallel to fiber direction		13.4 ± 1.1	0.29 ± 0.06
					Perpendicular to fiber direction		5.7 ± 1.1	0.10 ± 0.06
Box turtle (*Terrapene carolina*)[2]	**Rib**	Dorsal cortex		Dry	Cross-section	Load ≈9 mN (shallow indents)	~24	~1.1
		Cancellous interior					~18	~0.8
		Ventral cortex					~24	~1.1
Snapping turtle (*Chelydra serpentina*)[3]	**Keratin scutes**	Waxy surface		Dry	Cross-section	Depth ≈200 nm (shallow indents)	2.03 ± 0.18	0.07 ± 0.02
		Semi-waxy layer					8.25 ± 1.71	0.21 ± 0.03
	Rib	Ceramic-type dense layer					22.15 ± 1.99	0.52 ± 0.07
		Carbonaceous lamellae/fibrous structure					0.47 ± 0.07	0.05 ± 0.007
		Dense carbonaceous lamellae/fibrous structure					1.48 ± 0.35	0.07 ± 0.02
		Matrix (50%–60% porous).					11.34 ± 0.83	0.25 ± 0.02

strength across the boney teeth, while in the red-eared slider turtle the perisuture exhibits graded composition (mineral content) facilitating gradation in mechanical properties.

Furthermore, collagen is an organic polymer and as such exhibits viscoelastic properties such as stress relaxation and creep. Hence, to better characterize the suture behavior and the carapace in general, further time-dependent mechanical investigations are required.

3.3. Keratin scutes

The turtle shell is entirely covered with an epidermal keratinous coating which in practice is the first barrier against loads (Fig. 1). The epidermis is connected to the underneath bone through the dermis layer. In the carapace, the collagenous dermal layer extends from one suture to another, attaching the keratinous epidermis to the underneath dorsal bone (Fig. 2f-g). The scutes covering the carapace possess an approximately planar geometry. However, the boundary regions between adjacent scutes, termed hinges (Alibardi and Thompson, 2006) or sulci (Magwene and Socha, 2013), exhibit a folded geometry and usually lie over thinner bone regions displaying small channel-like depressions (Fig. 2h-l). In these hinge regions β-keratins proliferate (Alibardi and Thompson, 2006). While in the turtle carapace most of the nano-fibrils possess β-pleated sheet architecture, α-helix fibrils having coiled morphology are also present, but mostly in the inner layers of the laminate (Alibardi and Thompson, 1999; Alibardi, 2002).

The micro-structure of the keratin scutes resembles a laminate with many sub-micron layers (Fig. 2j-l). As mentioned earlier, each sub-layer of the laminate may be viewed as a fiber-matrix sheet where randomly-oriented nano-size stiff fibrils reinforce an amorphous and heterogeneous pliant matrix (McKittrick et al., 2012). The high allocation of sulfur (compared to the nearby dorsal bone) observed by EDS mapping (Achrai and Wagner, 2013) suggests that additional stiffening and hardening is likely achieved through cross-linking by disulfide bonds of abundantly-present cysteine residues (McKittrick et al., 2012). Indeed the keratinous epidermis exhibits high stiffness ($E_{dry} \approx 4$ GPa) and hardness ($H_{dry} \approx 0.2$ GPa) in comparison to mammalian skin tissues (Pailler-Mattei et al., 2008), comparable to other epidermal keratinous appendages such as nails (Farran et al., 2009), hair (Wei et al., 2005) and feathers (Bonser and Purslow, 1995). Under wet conditions the properties expectedly decrease ($E_{wet} \approx 1$ GPa, $H_{wet} \approx 0.03$ GPa), but to a lesser extent than for unmineralized collagen fibers. This is probably due to the presence of the nano-fibrils in the keratinous composite which are less prone to permeation of water molecules, avoiding disruption of their internal bonds.

Additionally, a small amount of calcium is observed as well (Achrai and Wagner, 2013). Yet, its structural form (e.g., crystalline or part of metallo-organic complex) and influence on the mechanical properties needs further investigation. The occurrence of calcium could be related to the dermal connective tissue linking the keratinous sheets to the underlying bone involving partly mineralized collagen fibers emanating from the dorsal bone and anchoring it to the keratin coating (Alibardi and Thompson, 1999).

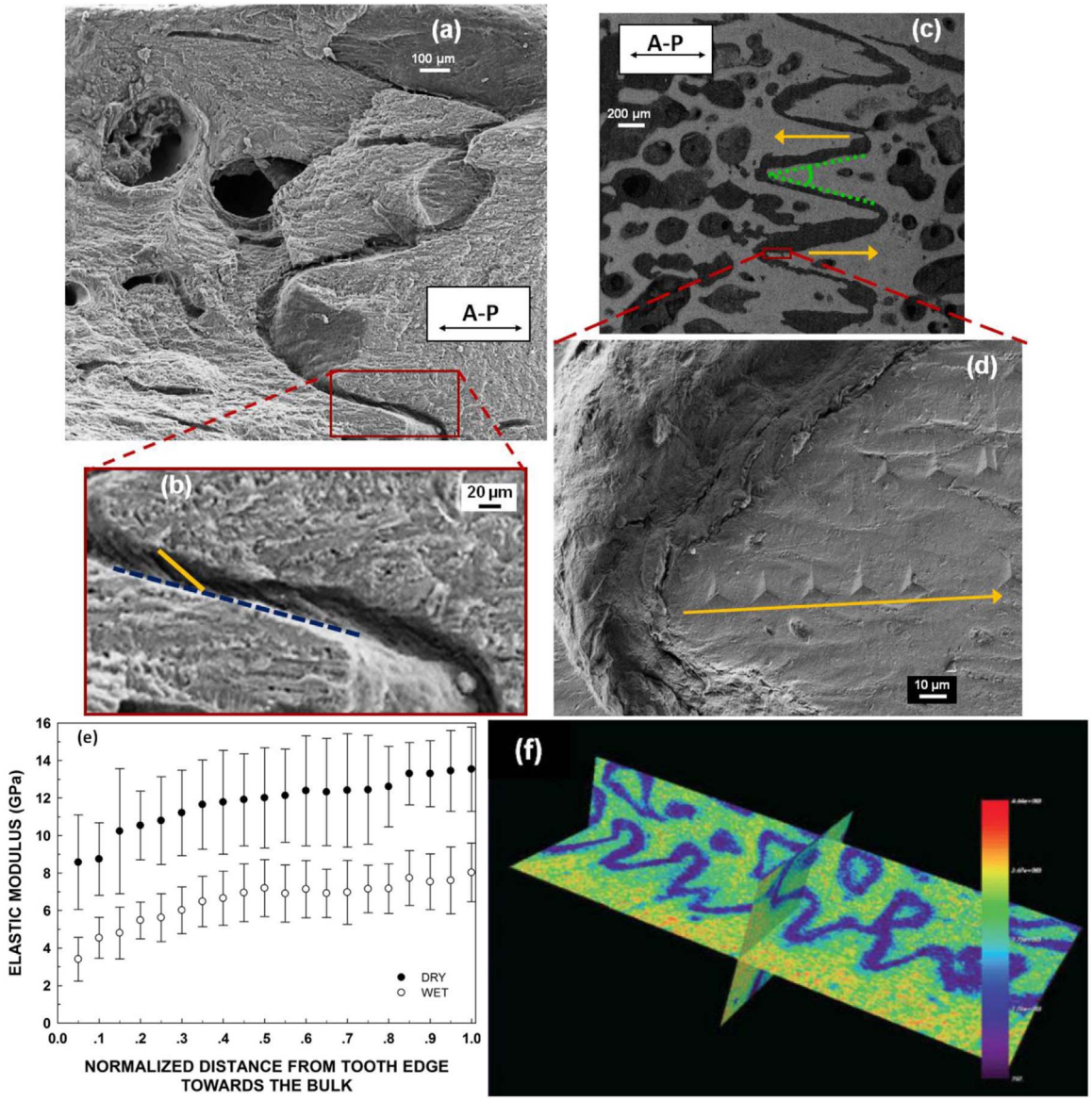

Fig. 4. (a) SEM fractograph of a saggital surface of a broken suture specimen, showing fibers organized roughly parallel to the A-P axis. (b) Inside the suture fibrils appear to be aligned at an angle to the suture path. The blue dashed line indicates the suture wake while the yellow line follows the fibril direction. (c) Backscattered electron image of the perisuture. The suture is seen as a black curly line and is clearly unmineralized. A representative tooth angle, $2\theta \approx 20°$ is indicated in green (d) Magnified (topological) image showing the interface between a suture and a bony tooth edge. In (c) and (d), the indentation course is indicated by the yellow arrows. (e) Plot of the mean elastic modulus of dry (solid squares) and wet (open squares) samples versus the normalized distance from the tooth edge towards the bulk, showing monotonic increase in stiffness when approaching the bulk bone from the tip edge. (f) Mineral distribution in the suture area obtained by segmentation of CT reconstructed scans. The red color indicates high concentrations, while the blue colors indicate no minerals (the color bar provides the bone mineral density in mg cm^{-3}). Graded increase in mineral content is clearly visible when approaching from the unmineralized suture towards the bulk bone, coinciding with the trend depicted in (e). Figs (a-e) and (f) were adapted with permission from (Achrai and Wagner, 2013) and (Krauss et al., 2009), respectively.

3.4. Summary of the microscopic features

The illustration in Fig. 5 summarizes the microscopic features of the rib and suture of the red-eared slider turtle carapace, showing the layered structure of the rib and the graded properties within the perisuture and the rib. Interestingly, the keratin scutes, the first line to protect against a predatory attack, is softer but tougher than the underlying dorsal bone. This type of layering, although less common in nature and synthetic armors, is crucial for proper impact shielding qualities of the carapace as will be shown in Section 5.1. In the next section we show how rib and suture specimens respond to quasi-static compression and bending loads, while taking into account their microscopic properties.

4. Quasi-static mechanical behavior

4.1. Compression

The compressive behavior of dry ribs taken from carapaces of the box turtle (*Terrapene carolina*) was evaluated by compression tests and finite element analyses (Damiens et al., 2011; Rhee et al., 2009). A unique stress-strain behavior akin to cellular solid materials was observed (Fig. 6a). This tri-region plot was attributed mainly to the foamy interior, depicting an initial linear elastic part involving bending of the trabeculae forming the foam, followed by a plateau corresponding to buckling, yielding and fracturing of the trabeculae, and a final linear densification stage of the fractured foamy interior (Ashby, 1983; Gibson, 2005). The latter stage showed a positive correlation of the absorbed energy (i.e., toughness) with the applied strain-rate, while the other regions showed

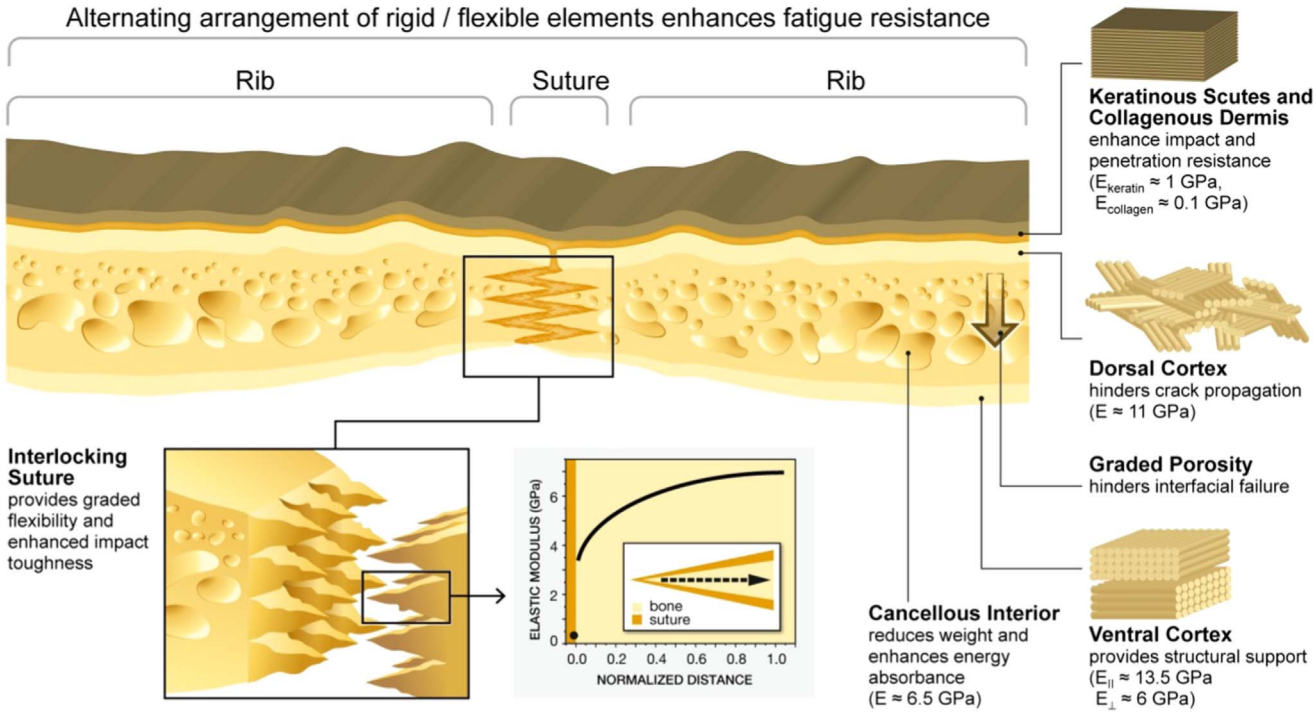

Fig. 5. Schematic showing the various microscopic features of the turtle carapace, including the rib layered structure, the perisuture and keratin scutes. The elastic moduli shown were calculated from nanoindentation measurements performed under wet conditions, reflecting physiological conditions.

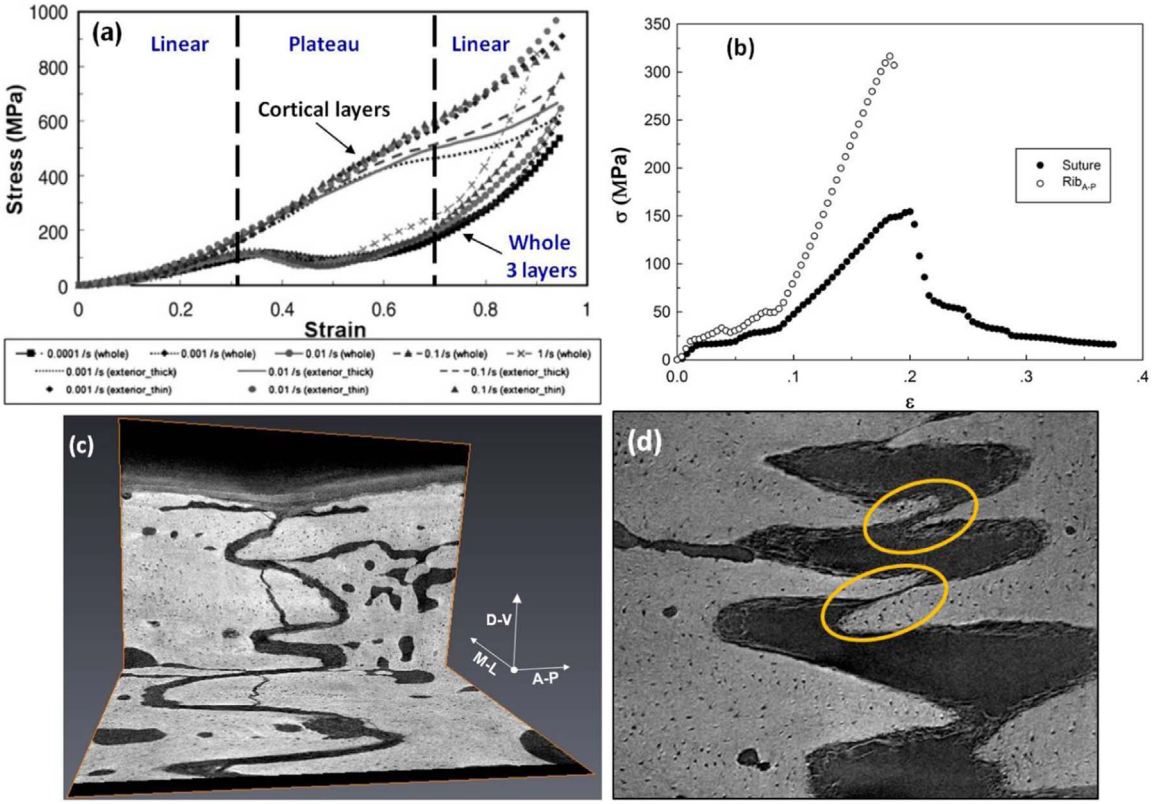

Fig. 6. (a) Representative quasi-static compressive performance of dry ribs taken from carapaces of the box turtle (*Terrapene carolina*). The specimens, containing the whole three layers, or alternatively only individual cortex layer, were tested under various strain-rates. Specimens containing the whole three layers show a unique deformation behavior involving a pronounced plateau region, corresponding to buckling and fracturing of the trabeculae forming the cancellous interior. (b) Representative flexure stress–strain curves of rib and suture specimens (both at low span-to-depth, SDR ≈ 4) taken from the carapace of the red-eared slider turtle. Although the suture is more compliant and weaker, it is reasonably tough and ductile. (c-d) Post-testing μCT imaging showing that some of the boney zigzag tips are (c) broken while others are (d) curved. The bent tips correspond to the local graded stiffness (measured by nanoindentation) that promotes higher degree of flexibility to the perisuture. Torn unmineralized collagen fibers are also visible in (d). Figs (a) and (b-c) were adapted with permission from Rhee et al. (2009) and (/Achrai et al. (2014), respectively.

strain-rate independency. This implies that the CI region may function, in part, to promote toughness enhancement under high strain-rate compressive loads, such as those encountered during predatory attacks or falls. In contrast to whole rib specimens, the compressive behavior of specimens containing only the cortex layers involved a standard linear elastic curve followed by a short yielding region until failure. The experimental results agreed fairly well with finite element analyses which included constitutive modeling of each region of the tri-phase stress-strain plot. Thus, it is reasonable to assume that the foamy (cancellous) region provides additional toughness to the boney regions of the carapace, acting as a cushion upon blunt (smashing, falling) as well as sharp (biting, clawing, pecking) compression loads.

4.2. Bending

During its lifetime, a turtle requires protection against high stress bending loads as well as against local compression (indentation). This is because the ribs (and the attaching sutures), comprising most of the carapace, are strongly fused to a thicker boney frame made of the vertebrate and the peripheral bones (Figs. 1b, 2a). Therefore, by contacting a predator tooth, claw or beak, or alternatively a stone, the bulk region will most likely undergo bending along with indentation. It is thus crucial to evaluate the bending performance of the turtle carapace. Thus we next elaborate on the quasi-static bending performance of the rib and the suture, followed by the evaluation of their dynamic behavior.

4.2.1. Rib

Rhee et al. (2009) measured a bending modulus of ~7 GPa for dry rib specimens extracted from the carapace of the box turtle (*Terrapene carolina*). Later on, Achrai et al. (2014) employed a combined experimental-analytical approach to evaluate the bending and shear moduli of dehydrated rib specimens taken from the red-eared slider turtle carapace. The approach also considered experimental limitations such as low span-to-depth ratios (SDR) of rib specimens (due to anatomical constraints) which in practice yield much lower bending moduli (~3 GPa) due to induced shear stresses along with bending stress. The authors showed how the bending modulus of the whole rib is dependent on the microscopic morphological and mechanical properties of each of its main four component layers. For these calculations the authors used Eq. (1), in which the flexural rigidity (EI) of the rib is a function of the moduli of the different sub-layers and their thicknesses (measured by electron microscopy), expressed via the parallel axis theorem. Eq. (1) is a simplified form of a degenerated classical laminate analysis calculation, see Appendix A in Achrai et al. (2014):

$$(EI)_{rib}=\Sigma E_i *(I_i+A_i r_i^2) \quad (1)$$

where E_i, I_i $(=wd_i^3/12)$ and A_i $(=wd_i)$ are the modulus, area moment of inertia and cross-sectional area of the ith layer (where i=DC, CI, VC-UPPER or VC-LOWER), respectively, and r_i is the distance from the mid-plane of the ith layer to the neutral plane of the rib. This was accomplished by testing specimens containing individual cortex layers, while the effective modulus of the foamy CI was estimated by cellular solid mechanics. The cortices showed bending moduli ranging between 5–11 GPa, depending on the direction of the boney fibers in each layer; bending in the long direction of the fibers yielded high stiffness (strength and toughness) values in comparison to bending the fibers in their transverse direction, coinciding with the micro-mechanical properties (Achrai et al., 2014). The bending modulus of each cortex layer was then used as input, along with the effective modulus of the closed-cell foamy region ($E_{CI} \approx 1.5$ GPa) which was estimated by using Eq. (2), taken from cellular solid mechanics:

$$E_{CI}=\rho_{CI}^3 * E_{sol} \quad (2)$$

where ρ_{CI} and E_{sol} are the relative density ($\rho \approx 0.5$, calculated from CT analysis) and the local microscopic modulus of the solid forming the foamy CI ($E_{dry} \approx 12.5$ GPa, measured by nanoindentation, Table 1, (Achrai and Wagner, 2013)), respectively. The analysis yielded bending moduli of ~7–9 GPa, for different carapaces, depending on the thicknesses of each layer in their laminate. This approach clearly shows how the compliant and porous cancellous interior provides a high specific stiffness to the whole rib: the area moment of inertia is maximized by placing the dense cortices away from the center and thus the overall stiffness is only slightly lower than the ones of the rigid cortices. With regard to reducing the overall weight of the carapace, the CI region also contains less mineral content than the cortices. Since the hydroxyapatite minerals are denser than the organic phase, the cancellous interior reduces the overall weight of the carapace by compositional means, along with the pronounced porosity.

In addition, the analysis also indicated an in-plane mechanical isotropy in the A-P and M-L directions, which is actually achieved through the anisotropic cross-ply morphology of the fibers in the double-layered ventral cortex. Furthermore, the shear modulus (~0.25 GPa) of the rib was found to be comparable to that reported for cancellous bone (Ashman et al., 1987; Goldstein, 1987), implying that shearing mainly occurs in the interior foamy region.

Rib specimens tested under wet conditions showed reduced strength and stiffness and increased post-elastic and failure strains, while toughness remained comparable to that of dry specimens.

It is important to note that the thin (~100 μm) keratin coating (including the dermis layer) has a negligible contribution to the overall bending stiffness of the rib. Nevertheless, the keratin scutes have a pronounced protective role as will be shown later (Section 5.1).

4.2.2. Suture

The compliant perisuture regions provide a degree of flexibility to the rigid boney carapace, which is essential for proper functioning of the animal, both under low- and high-stress situations. Krauss et al. (2009) showed by bending wet suture specimens (i.e., the interdigitating suture in the center flanked by neighboring ribs) that the zigzag morphology of the perisuture allows high deformation upon minor loads. The high compliance is essential for the reptile to carry out daily tasks (e.g., respiration, locomotion, feeding) which involve movement of the rigid ribs that constitute the majority of the carapace. The authors then showed that at higher loads, which may be encountered during predatory attacks, the specimens stiffen as neighboring bones become interlocked.

Later on, Achrai et al. (2014) showed that in comparison to the ribs, suture specimens possess lower stiffness and strength, but comparable toughness (Fig. 6b), probably due to the complex morphology and composition of the perisuture. After reaching their maximum stress (i.e., bending strength), the suture specimens fractured in a graded manner, by continuous breakage of the interlocked zigzag boney tips, until complete failure was reached. Indeed several broken tips were observed by post-testing μCT imaging (Fig. 6c). Nevertheless, x-ray tomography also revealed bent unbroken boney tips (Fig. 6d), likely as a result of the local graded stiffness (measured by nanoindentation), which is probably exploited for better interlocking of the suture upon bending. Post-mortem imaging also depicted torn unmineralized collagen fibers connecting two neighboring ribs prior to bending (Fig. 6d), likely providing an additional toughening mechanism. In a similar work, Magwene and Socha (2013) performed bending tests of suture and bone specimens taken from the plastron of several turtle species. However, neither the micro-properties of the bone specimens nor the effect of SDR were considered, and as a result the bending moduli of the bone specimens lied in a wide range, from ~2 to 12 GPa. Nevertheless, the measured stress-strain plots for the plastral bone and suture specimens displayed trends similar to the rib and suture specimens, respectively, that were cut from the carapace of red-eared slider turtles by Achrai et al. (2014).

5. Dynamic mechanical behavior

The primary function for which the turtle carapace has evolved is to protect the reptile from high-stress bending loads. These usually involve high strain-rate maneuvers exerted (i) by biting, clawing or

pecking during a predator attack, usually in a repetitive manner, or (ii) during falling or crushing against rocks at times of high tide or high current in streaming ecosystems. It is thus crucial to assess the dynamic bending properties of the turtle carapace, as shown below.

5.1. Impact performance

Common laminated armors, biological (Barthelat and Espinosa, 2007; Bruet et al., 2008; Yang et al., 2013) and synthetic (Collombet et al., 1998; Yadav and Ravichandran, 2003), usually comprise several layers in which the outer striking face is harder, stiffer and stronger than the more compliant backing plates. In such an arrangement the impacting projectile deforms upon hitting the outer layer, while the more compliant interior layer absorbs some portion of the kinetic energy (Tasdemirci et al., 2012). A drawback of such layer sequencing is that the hard outer layer may behave in a brittle fashion, particularly at high strain-rates, and thus undergo irreversible damage upon impact.

As shown in Section 3.3, similar to the osteoderms of alligators and the carapace of armadillos, the turtle carapace possesses a thin keratin coating which is softer but tougher than the stiff and strong dorsal bone just underlying. This sort of layer sequence, in which the striking face is softer than the stiffer backing plates, is less typical in biological and man-made armors, and may seem counterintuitive at first, especially since the thin keratin coating is practically ineffective in resisting quasi-static bending loads (Achrai et al., 2014). However, Balani et al. (2011) suggested that the "waxy layer", i.e., the keratin scutes, of the snapping turtle (*Chelydra serpentina*) is beneficial for stress relaxation, spreading the applied stress within the keratinous layer.

Recently Achrai et al. (2015) investigated the low-velocity impact response (~3 m s^{-1}, a rate relevant for natural conditions) of dry and wet rib and suture beam specimens, as well as specimens from which the keratin was removed. Remarkably, (hydrated) specimens containing the keratin coating absorbed three times more energy than the specimens without the keratin layer, even though the thickness ratio of the keratin coating (~0.1 mm) to the underneath bone (~3 mm) is only ~0.03. In addition, the structural integrity of the specimens following impact was partially maintained due to the adherence of the two opposing broken bone (or suture) pieces to the keratin coating (the so called 'adhesive tape analogy') which was stretched but not catastrophically (Fig. 7a-b,d-e). Pronounced delamination was indeed frequently observed in the keratin-collagen and collagen-bone interfaces. One should also bear in mind that the softer and tougher collagenous dermis, attaching the adjacent more rigid and hard keratin scutes and dorsal bone layers (Table 1), may spread the imposed stress and induce crack arrest by confining crack propagation within the soft interface region (Kolednik, 2000; Simha et al., 2003), in a way similar to the dentin-enamel junction in teeth (Imbeni et al., 2005). Another factor that may contribute to improving the absorbed impact energy is the waviness morphology of the interfaces, which may induce crack-path elongation and crack tip blunting (Li et al., 2012). In contrast to native specimens, specimens without the keratinous scutes completely shattered. Interestingly, dried specimens showed impact behavior (i.e., energy absorbance and structural integrity) akin to the "keratin-removed" specimens. The authors suggested that the failure strain and ductility of the keratinous tissue, which are enhanced by the plasticizing effect of water (McKittrick et al., 2012; Taylor et al., 2004; Wang et al., 2016), are crucial for proper impact resistance of the turtle carapace. Another toughening mechanism that may enhance the ductility of the hydrated keratinous tissue is the tension-induced α-helix to β-sheet transition in the keratin nano-fibrils (Fudge et al., 2003; Wang et al., 2016). This conformational transition initiating at the post-elastic region (of the stress-strain curve) was shown to induce further lengthening of keratinous materials by breaking hydrogen bonds in their α-helix coiled-coil structures and reforming the H-bonds to fit into the β-sheet structures.

With respect to the physiological functioning of the keratin scutes, they likely facilitate healing of the underneath bone that may be fractured by non-fatal assaults, enabling bone remodeling (Lyson et al., 2013) under adequate physiological conditions (e.g., maintaining a physical barrier, preventing pathogen infection). Similarly to the turtle carapace, the keratin coating of the beak of the Java finch (*Padda oryzivora*) was shown to provide adequate protection for the underneath brittle bone during impact loads such as biting (Soons et al., 2012).

Moreover, suture specimens absorbed three times more energy than the ribs, similar to the trends reported by Jaslow (1990) for suture and bone specimens taken from the skull of goats. The suture specimens exhibited rough fractured surfaces corresponding to a ductile failure (Fig. 7c-d), while the ribs possessed smooth broken surfaces corresponding to a brittle failure (Fig. 7a). In the turtle carapace and probably in the skull as well, the impact toughness of suture specimens is likely enhanced due to the complex morphology and composition of the perisuture. The interdigitating architecture assumingly causes meandering of crack propagation during untangling of the boney tips while dissipation of the impact energy is increased by the tough unmineralized collagen fibers spanning the suture.

5.2. High-stress fatigue behavior

Evaluating the fatigue behavior of the turtle carapace is imperative, as for any other structural material, but in particular because in nature the carapace may undergo repeated high-stress assaults exerted during biting, pecking or clawing of a predator (Magwene and Socha, 2013). This sort of cyclic loading arises because the tooth, beak or claw of a predator will usually not succeed in breaking the carapace in a single hit and the predator will most likely need to repeat this loading event many times (within a reasonable time frame). For that reason, the fatigue behavior of the carapace was recently examined by repeatedly bending hydrated rib and suture specimens at a frequency of 1 Hz (Achrai and Wagner, 2015). Subsequently, the authors constructed a stress-life (σ-N_f) plot, focusing on the high-stress region (i.e., 90%, 80% and 70% of the bending strength of each specimen type, Fig. 8a-b), which is more relevant to natural loading conditions. At very high stresses (90%) the ribs showed better durability ($N_{f\ \approx\ 75)}$ than the sutures which failed after only ~25 cycles. At lower stresses (80% and 70%), the number of cycles to failure only marginally increased for the suture specimens ($N_{f,70\%\ \approx\ 85)}$, while for the ribs N_f increased by a factor of 3 at 80% of specimen strength and by several orders of magnitude at 70% of specimen strength (reaching a number of cycles that is irrelevant in situations of predatory attacks).

The premature failure of the sutures, possessing similar number of cycles to failure at 90%, 80% and 70% of the specimen strength, may be linked to a swift untangling of the interdigitating boney tips, similarly to the unraveling of a zipper. In this manner, cracks originating from the weaker tensile side progress to the compression side through breakage and untying of the interlocked boney tips, and tearing of the unmineralized collagen fibers, until complete failure (Fig. 8c).

Since the turtle carapace exhibits a unique pattern of alternating rigid and flexible stripes corresponding to the ribs and sutures, respectively (Figs. 1b,2), another type of beam having a complex rib-suture-rib-suture-rib sequence was prepared (Fig. 8a). This was done to better comprehend the integrated response of the carapace under repeated high-stress loads. In the configuration of the complex specimens the moving anvil in the three-point flexure apparatus applied load at the midpoint of the central rib while the adjacent ribs (connected through the interdigitating sutures) rest on the supporting anvils. Remarkably, the complex specimens showed superior fatigue resistance compared to the suture and the rib specimens, needing ca. 320 cycles to fail when subjected to repeated high stress of 90% of the specimen strength. This implies a synergistic effect of the alternating arrangement of sutures and ribs along the carapace. At lower stresses

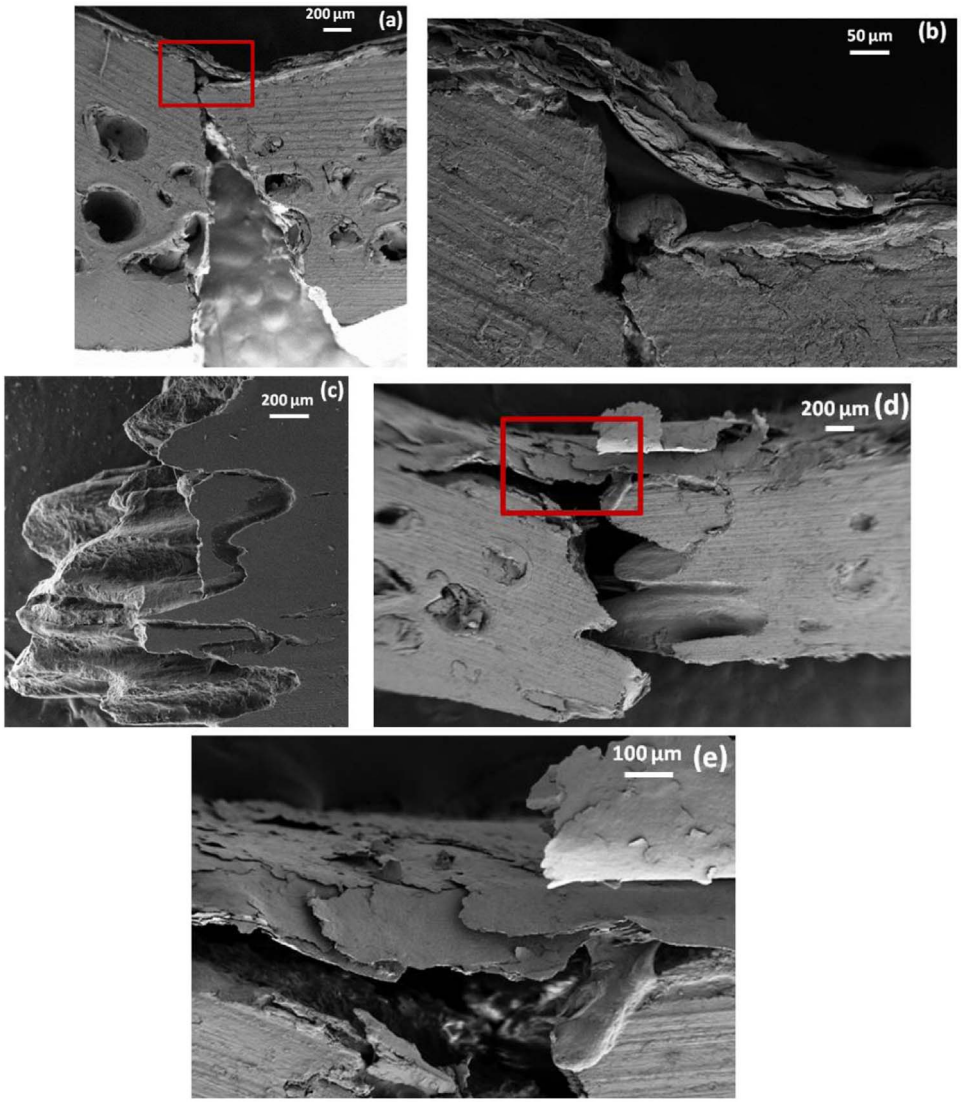

Fig. 7. (a) Representative SEM image of an impacted native rib specimen showing smooth fractured bone surfaces, corresponding to a brittle failure. The two facing broken bone elements are seen held together by the keratinous laminate coating. (b) Higher magnification showing the area marked by the red rectangle in (a). Delamination is observed at the keratin–collagen and at the collagen–bone interfaces. (c-d) Representative SEM images of impacted native suture specimens, showing rough fractured surfaces, corresponding to a ductile failure. In (d), the broken rigid zigzag elements are seen held together by the keratinous laminate coating. (e) Higher magnification showing the area marked by the red rectangle in (d). Delamination is observed at the sub-layers of the keratin laminate and at the keratin–collagen and at the collagen–bone interfaces. Figs (a-e) were adapted with permission from (Achrai et al., 2015).

(80% and 70%) the complex specimens retained their superior durability compared to the other specimen types. Nevertheless, importantly, it must be noted that the complex specimens possess intermediate bending strength compared to the stronger ribs and the weaker suture specimens. However, these values may not be fully trustworthy since the SDR of the complex specimens (~14) was higher than the ones of the rib and suture specimens (~8) due to morphological constrains (i.e., the distance between the sutures limits the available span).

Furthermore, two failure modes were observed for the complex specimens; about half of the specimens failed in one of the two suture regions and the rest failed in regions close to the perisuture where a thin cancellous necking zone, connecting the rib bulk with the suture, is present (Fig. 8d). The latter may be due to weak points in the complex specimens and probably in the whole carapace. The superior fatigue endurance of the complex specimens was attributed to the interdigitating morphology of the flexible perisutures, which likely enables rearrangement of the zigzag tips of neighboring ribs by allowing constrained movement. In this way, upon each loading cycle, reorganization of the tips is achieved, at least in part, through displacement of the unmineralized collagen fibers that span the suture. Eventually the specimens fail at the weakest points mentioned above. Importantly, since the peak stress is exerted mostly on the central rib, it is reasonable to assume that the suture sites are not stressed to their maximum bending stress and hence do not fail as early as in the suture specimens in which the peak stress is applied on the perisuture. Clearly, more investigations are required to understand the failure mechanism.

6. Whole carapace mechanics

Thus far specific regions (ribs, perisutures, keratin scutes) in the turtle carapace were comprehensively characterized, starting from their microscopic features to their macroscopic mechanical behavior. Correlations between the micro-properties and the macroscopic performances were then drawn for various loading conditions relevant to the protective functioning of the carapace.

Next, the mechanical performance of whole carapaces must be assessed. Several studies have addressed this issue (Fish and Stayton, 2014; Hu et al., 2011; Magwene and Socha, 2013; Polly et al., 2016;

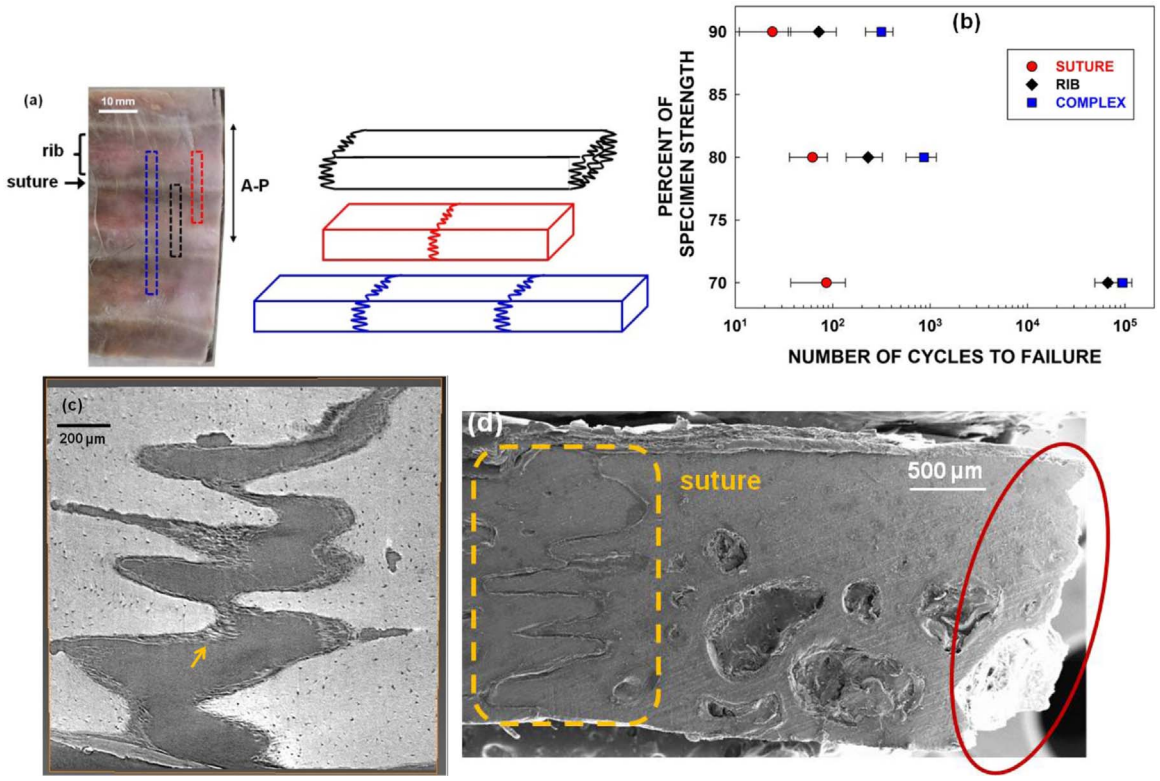

Fig. 8. (a) Ventral view of a carapace cut showing the alternating rib and suture elements. The anterior–posterior (A–P) direction is indicated. The dashed black, red and blue rectangles correspond to the schematic showing rib, suture and complex specimens, respectively. (b) Stress-life (σ-N_f) plot showing the fatigue behavior of rib, suture and complex specimens in the high-stress low-N_f region. The suture and complex specimens exhibit inferior and superior durability, respectively, in comparison to the rib. Error bars represent the standard deviation. (c) Post-testing CT slice of a suture specimen showing unlocking of the boney zigzag tips and rupture of the unmineralized collagen fibers (indicated by the yellow arrow) initially spawn the suture (and connected the two facing boney tips) prior to loading. (d) Post-testing SEM imaging of a complex specimen showing a typical failure region adjacent to the perisuture which consists of mostly thin cancellous bone. Figs (a-d) were adapted with permission from (Achrai and Wagner, 2015).

Stayton, 2009, 2011; Rivera and Stayton, 2011; Vega and Stayton, 2011), however only one contained experimental investigation (Magwene and Socha, 2013), whereas the others use modeling (mostly finite element simulations). We now review the main findings and insights that emerge from these works.

Many turtle species possess a carapace resembling a flattened dome adapted to reduce drag forces and increase hydrodynamic efficiency i.e. streamlining and swimming speed (the latter can reach ~1 m/s for the sea turtle (Luschi et al., 2001)). Terrestrial tortoises, on the other hand, usually exhibit heavy, bumpy and highly-domed carapace (Fig. 1a), which promotes the high strength needed to defend against predators that might attack during the reptiles' sluggish movement. Using finite element modeling, Rivera and Stayton (2011) pointed out that there appears to be a trade-off between the shell strength and its hydrodynamic efficiency, which is governed by the shell curvature (Fig. 9). They showed that flatter carapaces of the lotic river cooter (*Pseudemys concinna*) exert lower drag forces but are also weaker than the domed carapaces of the lentic bog turtles (*Glyptemys muhlenbergii*). They noted that such weakness can be overcome by increasing the shell size: doubling the size yields a four-fold increase in strength with negligible decrease in hydrodynamic efficiency. Later on, the positive correlation between strength and curvature was shown to be exploited by juvenile red-eared slider turtles, which possess a small partially-developed but highly-curved carapace, in comparison to the flatter, larger and fully-developed carapace of adult animals (Fish and Stayton, 2014). In this case, a geometrical feature (curvature) was assumed to compensate for the inherent low strength of the developing carapace due to inferior material properties (low carapace thickness, connectivity and degree of mineralization). Still, the survival rate in immature turtles (~0.18–0.35) is much lower than in adults (~0.76–0.98, (Congdon and Gibbons, 1990; Iverson, 1991)) due to efficient protection of their fully grown shells.

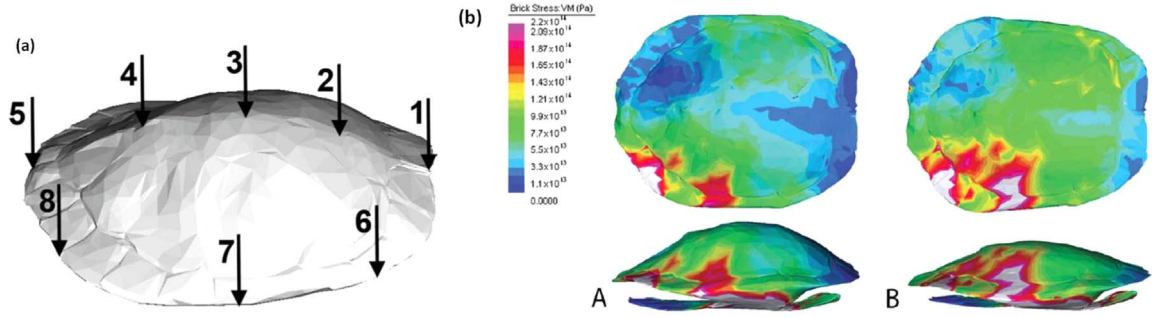

Fig. 9. (a) A representative carapace scan taken for finite element analysis showing eight different load cases (marked by arrows). (b) von Mises stress distribution maps calculated for load case 8, for turtles having (A) a high-dome carapace (lentic species) and (B) a low-dome carapace (lotic species). The color-coded stress scale shown at left reveals that a flatter carapace exhibits higher stresses. Figs (a-b) were adapted with permission from Rivera and Stayton (2011).

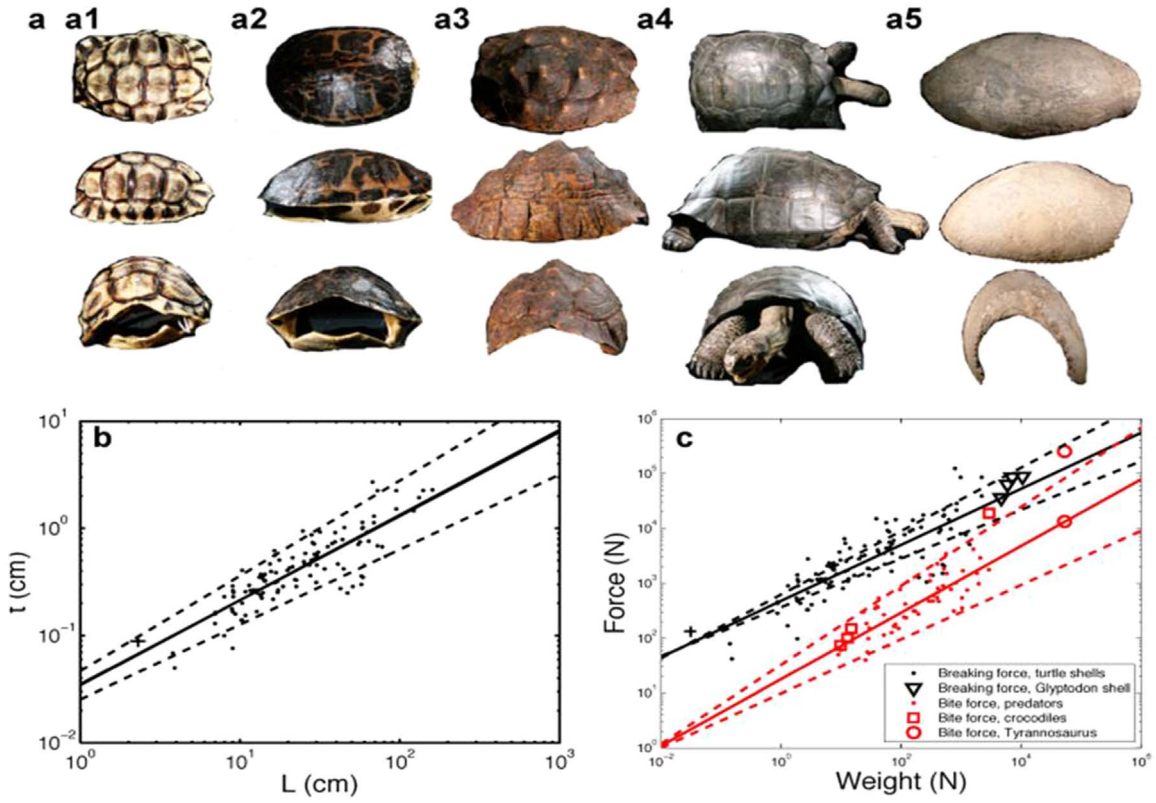

Fig. 10. (a) Turtle shells from 3–100 cm in diameter, here magnified to the same size, highlighting the similarity of their proportions. (a1) Angulate tortoise (*Chersina angulata*), L = 3.9 cm. (a2) Florida redbelly turtle (*Pseudemys nelsoni*), L = 28.5 cm. (a3) Leopard tortoise (*Geochelone pardalis*), L = 29.1 cm. (a4) Galapagos giant tortoise (*Geochelone nigra*), L = 58.8 cm. (a5) Shell of glyptodon, a prehistoric armored mammal, L = 130 cm. (b) The relation between turtle shell thickness t and length L. Solid lines indicate the best fit ($t = 0.04\ L^{0.8}$); dashed lines indicate the 95% confidence intervals for this fit. Characteristic errors of measurement are shown. (c) Bite force F_{pred} of predators (red) and bite resistance F of turtle shells (black) as a function of their body weights W. Solid lines indicate the best fits: $F_{pred} = 20\ W^{0.6}$, $F = 470\ W^{0.5}$; dashed lines indicate the 95% confidence intervals for this fit. Figs (a–c) were adapted with permission from Hu et al. (2011).

In another morphometrical study combined with elastic thin shell theory, Hu et al. (2011) measured the thickness (t) and length (L) of shells of many turtle species and drew a scaling law where $t \approx 0.04\ L^{0.8}$ (Fig. 10). The authors then suggested that the breaking force of the shell is ~40 times the bite force of predators having the same weight as the turtle. On the other hand, they concluded that a predator weighting ~200 times the turtle weight can successfully break the turtle shell, such as in the case of a ~360 kg alligator attacking a ~2 kg turtle.

The aforementioned morphometric studies involved finite element methods based on 2D digital camera images or 3D computer tomography scans of whole shells. These simulative investigations require several prerequisites which may overly simplify the complexity of the turtle shell and therefore hamper the accuracy of their results. The somewhat restrictive hypotheses used included the following: (i) Linear elastic behavior of the shell is assumed; In fact, the shell is a complex hierarchical composite structure consisting of viscoelastic elements (bone, unmineralized collagen fibers and keratinous tissues), and thus most likely behaves in a viscoelastic and plastic fashion, which should lead to deviations from the results (ii) The shell structure is homogenous and local material properties of the shell are neglected, including composition (e.g., mineral content, hydration state) and morphology (e.g., foamy regions, sutures). These material properties were shown earlier to govern the overall mechanical behavior of the shell and should be taken into account to obtain reliable predictions of its mechanical response. (iii) The shell was assigned an elastic modulus of 22 GPa [Rivera and Tayton, 2014], which is much higher than the range of bending and compressive moduli shown earlier (Achrai et al., 2014; Rhee et al., 2009). One should bear in mind that the high reduced elastic modulus obtained by nanoindentation in (Balani et al. (2011) and Rhee et al. (2009) was measured under dry conditions and on very small bone volumes, which highly overestimates the elastic modulus measured for macroscopic specimens (see Section 4). (iv) Element shapes in the finite element software were adjusted (e.g., an irregularly-shaped/elongated element was transformed into a cubic element), which may lead to less-precise results as well.

Nevertheless, some of the listed drawbacks may be overcome by utilizing simulative methods that have recently been developed, taking into account viscoelastic elements integrated within layered structures (Moita et al., 2013) and spatially-varying Young's moduli and porosity (Byrne et al., 2007).

As an example for inconsistency between the simulative and experimental results, a discrepancy is found between the FEM results published in Stayton (2009) and the experimental work reported by Magwene and Socha (2013). The modeling study suggested that the boney bridges connecting the carapace to the plastron are the regions containing the highest stress concentrations. However, other failure regions were identified by assessing the behavior of whole shells (which were not isolated from the reptile body) of several species of turtles (*Trachemys scripta*, *Malaclemys terrapin*, *Chrysemys picta, and Terrapene*) under compressive loads (Fig. 11a). Interestingly, most of the shells failed in their sulci (i.e., the boundary regions of adjacent scutes possessing thinner bone channels underneath) located in the lateral regions of the carapaces (Fig. 2h-l). It thus can be concluded that the material properties of such a complex hierarchical composite structure govern its mechanical behavior and better assumptions are needed to refine the modeling predictions.

In addition, most of the bone fractures were locally confined in the M-L orientation (usually restricted to one side of the carapace, Fig. 11b-c), probably because the soft sutures constrained cracks from propagating in the A-P direction, showing an additional benefit of the

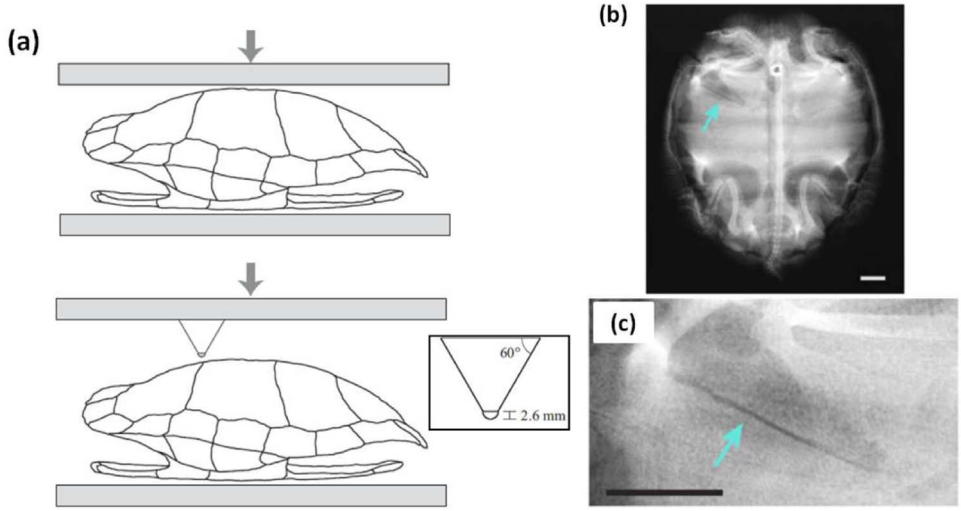

Fig. 11. (a) Schematics showing the experimental setup used for broad (top) and point (bottom) compression loadings of whole shells. The inset shows the geometrical features of the point loading apparatus. (b-c) Dorsal-view radiographs of the carapace of the painted turtle (*Chrysemys picta*) following broad compression tests, showing a macroscopic transverse crack, oriented in the M-L direction. Scale bars=1 cm. Figs (a-c) were adapted with permission from Magwene and Socha (2013).

alternating rib-suture arrangement. Only two out of 14 shells failed by (lateral) suture rupture. It is reasonable to assume that for the remaining twelve shells, the sutures probably provided a certain extent of reversible displacement of the boney regions within the carapace (and the whole shell) until fracture occurred in the more brittle (peripheral) bones. Another interesting finding was that smaller turtle shells possessed larger deformations, consistent with the finite element simulations reported by Fish and Stayton (2014). The observed large compliance is most likely achieved since these turtles were not fully developed and thus their shell was not fully ossified in terms of bone thickness, mineral content and fibrillar orientation. The experimental work also included a point loading fixture designed to simulate a predator tooth (Fig. 11a), inducing high local stress concentration. All of the carapaces subjected to the point loading failed locally with fractures surrounding the area of the applied load. Much work is still required to fully understand the resistance of the carapace to indentation and puncture situations.

7. Resistance of the carapace against penetration loads

In a recent study (Shelef and Bar-On, 2017) the resistance of dried carapace specimens to quasi-static penetration loads was studied by means of micro-indentation tests combined with finite element modeling. The simulations included a “soft-softer-hard” layer sequencing corresponding to the keratinous epidermis-collagenous dermis-dorsal bone layers. The authors suggested that a “bumper-buffer” toughening mechanism is involved, in which (i) the outermost keratin layer serves as a bumper by adsorbing part of the indentation energy, and (ii) the intermediate softest collagenous layer disperses the absorbed energy by plastic deformation. It was concluded that the boney carapace is further protected from sharp assaults (that may be induced during a predatory attack) by the addition of the soft intermediate dermis layer in-between the keratin coating and the dorsal bone. Additionally, the effect of hydration, which was addressed in the simulations by applying the wet moduli values of each layer, yielded deformation behaviors similar to the ones obtained under dry conditions. Nevertheless, to fully understand the influence of hydration, further experimental investigation performed under wet conditions is required. In addition, the viscoelastic characteristics that are typically promoted by hydration are anticipated to play a crucial role primarily under dynamic high strain-rate penetration loads (such as those imposed during predatory attacks) rather than under quasi-static deformations.

8. Integration of the sub-regions into an efficient carapace

An efficient mobile armor, such as the turtle carapace, should possess high stiffness, strength and toughness, and also be as light as possible. While the first two properties are usually compatible, they are often incompatible with high toughness. To overcome this drawback, nature has developed sophisticated design strategies for the turtle carapace, which sprawl over several length-scales and combine special arrangement of alternating rigid and flexible elements, three-dimensional interlocking morphology, functionally graded material properties and layered structuring (Fig. 5). We now review the key insights of how the turtle carapace achieves the aforementioned desired properties:

8.1. Ribs provide stiff, strong and light-weight structural support

The high specific stiffness and strength of the ribs provide structural support to the carapace, while each of the ribs’ sub-layers exhibits a different mechanical function: The ventral cortex possesses a plywood structure with two orthogonal parallel-fibered sub-layers oriented in the M-L and A-P directions. This micro-assembly is useful for structural support in the mentioned orientations where the fibrils are loaded in their longitudinal direction, in which their stiffness and strength are the highest. This sort of loading condition may arise during a predator attack, during which the carapace will most likely undergo bending and the VC layer will experience tension, and will thus provide maximal bi-lateral (in-plane) resistance (i.e., structural support in the A-P and the M-L directions). It is also conceivable (but yet unproved) that the 0°/90° orthogonal configuration of the ventral cortex contributes to the formation of the convexity of the rib via residual stress buildup.

In contrast to the VC layer, the dorsal cortex exhibits structural characteristics assumed to be designed for coping with outside aggression (biting, clawing, pecking, and so on). The dense DC layer displays a randomly oriented osteonal network (on the meso-scale) embedded in an interwoven fibrillar array, resulting in a disordered local structure. The absence of a preferred fibrillar and osteonal alignment may result in crack propagation redirecting (Raabe et al., 2005). Multi-scale disorder hampers sub-micron crack initiation within the fibrillar matrix and the twisted plywood-like concentric lamellae (Peterlik et al., 2006), and also confines the spread of larger (micro-size) cracks within the osteonal network (Gupta and Zioupos, 2008). Consequently, the dorsal cortex provides a dense, rigid and disordered boney barrier

designed to withstand sharp assaults by preventing developing cracks from further penetrating the carapace and becoming catastrophic.

In contrast to the dense cortices, the foamy core enables reduction of weight due to low relative density ($\rho \approx 0.5$) and low mineral content (~50 wt%, compared to ~60 wt% of the cortices), with minimum mechanical cost. This is accomplished because the area moment of inertia, which governs (along with the elastic modulus) the bending stiffness (EI), is only minutely affected (Section 4.2). Additionally, the cancellous interior, viewed as a cellular solid material, absorbs the mechanical energy, acting as a cushion (Ashby, 1983; Gibson, 2005).

The sandwich-like structure of the rib resembles artificial rigid skins/foamy core assemblies found in various man-made applications where stiff and light materials are needed, e.g., as structural elements of vehicles and airplanes. An additional resulting property of this sandwich structures is buoyancy, which is indeed utilized by turtles (Krauss et al., 2009) and also in man-made surfing boards (Chimiak, 1996). Nevertheless, dissimilarly to synthetic materials, the turtle carapace rib exhibits graded porosity when approaching the foamy CI region from the dorsal cortex. This architectural motif, which is highly sought-after in man-made materials, is assumed to hinder numerous modes of interfacial failure (e.g., face wrinkling, cell buckling) (Petras and Sutcliffe, 1999).

8.2. Sutures and keratin scutes enhance impact resistance

The sutures and the thin keratin coating greatly improve the impact toughness of the carapace through two different mechanisms: (1) the sutures' composition and morphology enable high energy absorption, likely due to the viscoelastic dissipative nature of the interconnecting unmineralized collagen fibrils, and to the interlocking configuration of the boney tips which lead to meandering of crack propagation. In addition, the enhanced flexibility of the perisuture due to the graded composition and the corresponding graded stiffness and hardness of the boney zigzag tips allow improved interlocking of the perisuture which prevent breakage of the tips at lower stresses. (2) the thin and ductile keratinous coating, which is composed of many sub-micron layers, and the underneath unmineralized fibrillar collagen dermis interlayer, undergo debonding at the keratin-collagen and collagen-bone interfaces and within the keratin laminate as well. In addition, the waviness of these interfaces promotes crack path elongation and crack tip blunting (Li et al., 2012). These result in delamination events which assist in dissipating the impact energy and maintain structural integrity by effectively binding the broken boney regions ("adhesive tape" analogy). Additional toughening may be realized by the "soft-softer-hard" stacking sequence of the keratin coating-collagenous dermis-dorsal cortex. This morphological feature may lead to lateral spreading of cracks, preventing propagation into the more brittle dorsal bone, and assist in stress dissipation (Shelef and Bar-On, 2017; Kolednik, 2000; Simha et al., 2003).

Note also that since the keratin coating is more than an order of magnitude thinner than the whole carapace, its effect on the bending stiffness is negligible. Thus the impact toughness of the carapace is enhanced without stiffness deterioration.

8.3. Macroscopic alternating structural arrangement enhances fatigue resistance

The carapace comprises rigid ribs interconnected by flexible collagenous sutures, resulting in a unique alternating-stripes pattern. Although individual sutures exhibit inferior fatigue resistance, the repeating rib-suture configuration provides superior resistance to cyclic loads, which also outperforms the ribs. This synergistic effect of the rigid and flexible elements is presumably achieved due to rearrangement of the zigzag tips of neighboring ribs at the pliant perisutures upon each loading cycle, through displacement of the unmineralized collagen fibrils spanning the suture. Then the complex specimens reorganize and are "ready" for another loading event. Eventually the specimens fail at the weakest point, which is usually either a thin cancellous rib region adjacent to the suture, or the interdigitated suture itself. Additionally, the unique alternating pattern contributes to confining cracks from propagating in the anterior-posterior direction, because the laterally-oriented soft sutures spread the imposed stress and reorient developing cracks in the M-L direction.

Moreover, the carapace bulk consists of alternating stripes of wide (~10–20 mm) rib and narrow (~1 mm) suture elements (Figs. 1b,2a), thus, statistically, upon repeated predator attacks, the predator tooth or claw will most probably hit the boney region and not a suture in its center. This naturally-occurring loading situation resembles the complex specimens test setup, which, as discussed, is advantageous upon flexural high-stress cyclic loadings, exhibiting increased durability.

The schematic drawing shown in Fig. 5 summarizes the main features of the carapace and their contribution to its overall mechanical performance.

9. Bio-inspired designs

The complex hierarchical multi-motif architecture of the turtle carapace and its corresponding mechanical functioning could be a source of inspiration for engineers and researchers in designing innovative protective materials. Yet, although nature, in particular, turtles, utilize a self-assembly bottom-up approach to construct their shells (Gilbert et al., 2001), it is still a challenging obstacle to produce synthetic counterparts with such complex morphologies and compositions.

First attempts in achieving this ultimate goal have nevertheless already been carried out (Achrai et al., 2015; Yu et al., 2016; Zhu et al., 2016). Specifically, the positive effect of the thin keratin coating on the impact performance of the whole carapace has recently attracted much attention. Achrai et al. (2015) showed that coating thick hard and brittle substrates (e.g., alumina, glass) with a thin layer of ductile polymer (e.g., polyvinyl alcohol, polyvinyl butyral, polycarbonate) leads to improved impact resistance of the substrate. The synthetic analogues, having coating-to-substrate thickness ratios similar to the biological specimens, were found to possess an impact performance, i.e., impact toughness and structural integrity, similar to the carapace (Fig. 12a-b). Yet, the synthetic specimens absorbed lower impact energy presumably due to their simple planar coating-substrate interface which also lacked a softer intermediate layer and anchoring fibers that hold together the adjacent coating and substrate layers. Importantly, the behavior of substrates coated with a brittle polymer (PMMA) was akin to uncoated specimens, emphasizing the role of ductility of the coating, a proven crucial factor in biological specimens (Section 5.1) (Achrai et al., 2015). The phenomenon shown above has recently been exploited in man-made structures such as military vehicles and buildings requiring high endurance against blasting events (Raman et al., 2012; Samiee et al., 2013; Tekalura et al., 2008). In these cases, the supporting structures are being sprayed over with an elastomeric polyurea layer which attenuates the compressive shock waves generated by the blast or the impacting projectile, and protect the structures from shattering (Roland et al., 2010) (Fig. 12c). Although the toughening mechanisms involved are not entirely understood, they involve pronounced energy dissipation within the elastomeric layer due to strain-induced rubbery-to glass state transition (Bogoslovov et al., 2007). For further details about blast mitigation coatings, the reader is referred to a recently-published review by Chundawat et al. (2016).

In a rather different approach, the general scheme of laminated structure of the keratin scutes laid over a boney layer was recently imitated by sintering Ti and Al foils into diffused metallic laminates which in turn were fused onto an underlying SiC fiber-reinforced titanium matrix (Zhu et al., 2016; Yu et al., 2016). The authors showed that the resulting hybrid composites became more ductile, exhibiting

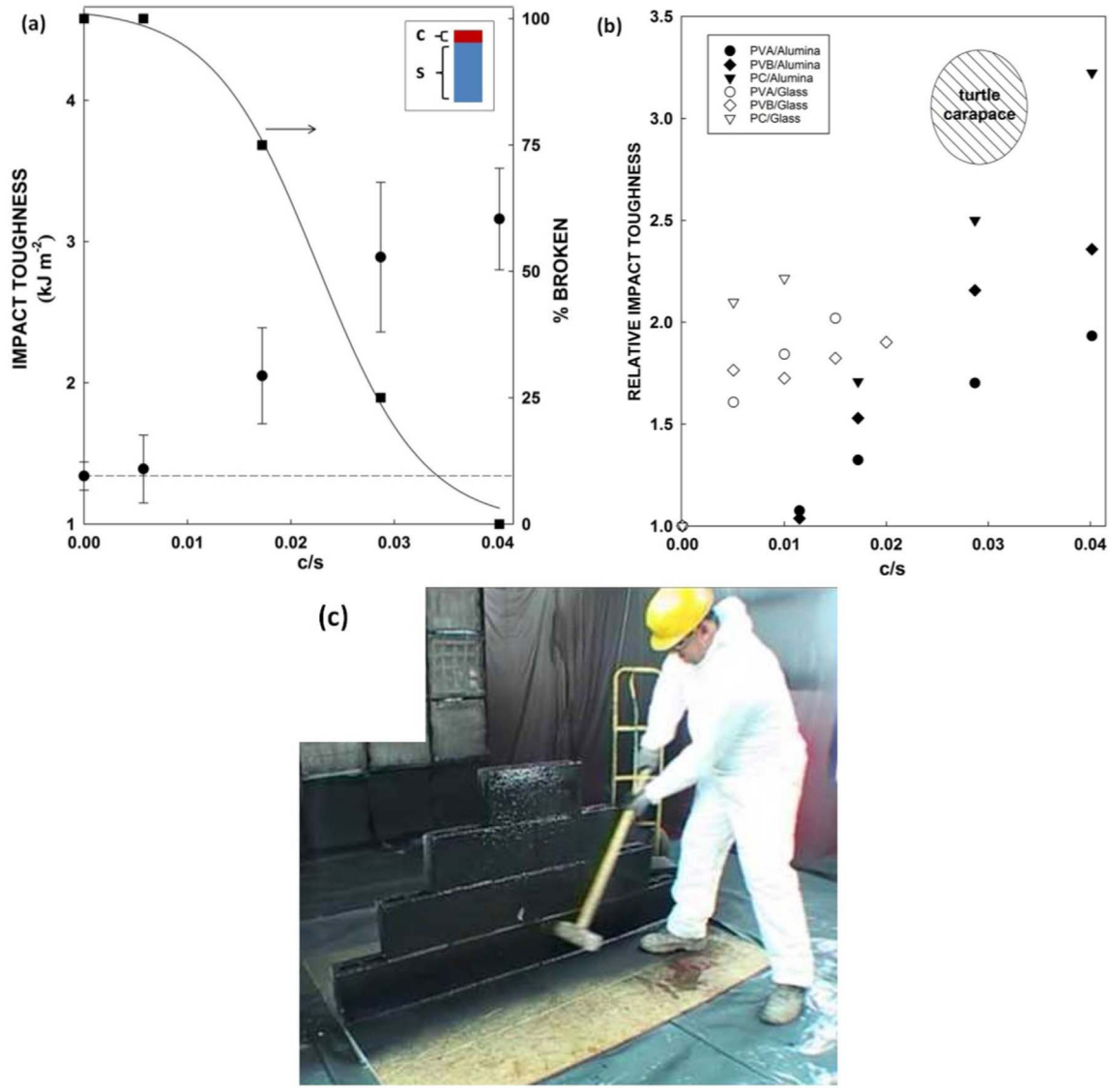

Fig. 12. (a) Plot of the impact toughness (circles) of PVB/alumina laminates and of the fraction of failed specimens (squares) as a function of the coating/substrate thickness ratio c/s; see inset. The dashed horizontal line, drawn as a reference, represents the impact toughness of pristine alumina. Note that for representative purposes, the impact toughness values are averaged over the total of broken and unbroken specimens (only a negligible impact toughness difference between the broken and unbroken specimens was obtained). (b) Plot of the relative impact toughness (impact toughness of the coating/substrate laminates divided by the impact toughness of the pristine substrate) of coating/substrate structures as a function of c/s. Note that beyond c/s ≈ 0.015 (for the glass laminates) and c/s ≈ 0.03 (for the alumina laminates), catastrophic failure was not observed (i.e., the polymeric coating preserved the integrity of the specimens). The ellipse area, drawn for comparison, represents the range of results obtained for turtle carapace specimens. (c) Demonstrative image showing a polyurea-coated brick-wall which remains intact after being hit by a sledgehammer. Figs (a-b) and (c) were adapted with permission from Achrai et al. (2015) and GLS Coatings LTD, respectively.

failure strains (~4.2%) comparable to the inter-metallic ones and higher than that of the SiC-fiber reinforced Ti-matrix (~3%). Crack deflection by the inter-metallic laminate was observed, protecting the underneath fiber-reinforced matrix. In addition, the stiffness and strength of the hybrid structures showed values in-between those of the stiffer and stronger fiber-reinforced matrix and the weaker metallic laminate.

Other motifs in the turtle carapace are yet to be realized by synthetic means. Bio-inspired rigid structures incorporating flexible suture elements have recently been reported, but the morphologies of the sutures in those works exhibit mainly the peg and socket and the overlapping motifs. These are usually found in fish scales (Browning et al., 2013; Vernerey and Barthelat, 2010; Zhu et al., 2012) and allow a higher degree of compliance, which is relevant, for instance, in human shields necessitating flexible maneuvering. Still, the complex inter-digitating morphology of the carapace suture is yet to be demonstrated by synthetic means.

The turtle carapace also exhibits functionally graded structural elements such as graded porosity and graded mineralization, both leading to gradation in mechanical properties such as local microscopic hardness and stiffness, and macroscopic stiffness, in the former and latter examples, respectively. Indeed functionally graded composites have gained much attention in recent years (Shen, 2016), especially in aerospace industries, as thermal barrier coatings, to improve resistance to wear, corrosion and heat (Schulz et al., 2003), and in bio-medical applications as bone grafts (Askari et al., 2012; Sola et al., 2016)). Yet, the majority of work reported in the literature is of a theoretical nature, while the fabrication of applicative functionally graded materials is still very limited (Shen, 2016; Sola et al., 2016; Yang, 2015). Though graded porosity is indeed produced in orthopedic implants, to the best of the authors' knowledge, dense skin/foamy core sandwich materials possessing graded porosity, and structures possessing rigid and flexible elements attached together by a graded and morphologically-complex interface, are yet to be manufactured.

10. Outlook

A large body of work concerning the structure-mechanical function of the turtle carapace has been presented in the current review. Much is left to explore, however, mainly in the characterization of the viscoelastic properties of the carapace sub-regions, including the keratinous scutes and the collagenous sutures. Both possess a pronounced time-dependent mechanical response and it is crucial to comprehensively understand how the biological armor performs, specifically under higher strain-rates. In addition, evaluating the behavior of the whole carapace, including its resistance to local puncture and blunt loads, by experimental means, is still lacking, specifically under conditions resembling natural high stress and strain-rate loading situations encountered by turtles.

Although several theoretical works have modeled the carapace behavior by finite element means, further refinements which consider, for instance, its complex micro-structure are required to better appreciate the mechanical response of the turtle carapace.

Acknowledgements

Thanks are due to GLS Coatings LTD for kindly providing the photograph included in Fig. 12c. This research was supported by The Israel Science Foundation (grant No. 727/14) and by the generosity of the Harold Perlman family. We also acknowledge support from the G.M.J. Schmidt Minerva Centre of Supramolecular Architectures. H.D.Wagner is the recipient of the Livio Norzi Professorial Chair in Materials Science.

References

Achrai, B., Wagner, H.D., 2013. Micro-structure and mechanical properties of the turtle carapace as a biological composite shield. Acta Biomater. 9 (4), 5890–5902.
Achrai, B., Bar-On, B., Wagner, H.D., 2014. Bending mechanics of the red-eared slider turtle carapace. J. Mech. Behav. Biomed. Mater. 30, 223–233.
Achrai, B., Bar-On, B., Wagner, H.D., 2015. Biological armors under impact-effect of keratin coating, and synthetic bio-inspired analogues. Bioinspir. Biomim. 10 (1), 0160.
Achrai, B., Wagner, H.D., 2015. The red-eared slider turtle carapace under fatigue loading: the effect of rib-suture arrangement. Mater. Sci. Eng. C. 53, 128–133. http://dx.doi.org/10.1016/j.msec.2015.04.040.
Alibardi, L., 2002. Immunocytochemical observations on the cornification of soft and hard epidermis in the turtle Chrysemys picta. Zool. (Jena) 105 (1), 31–44.
Alibardi, L., 2013. Ultrastructural immunolocalization of alpha-keratins and associated beta-proteins (beta-keratins) suggests a new interpretation on the process of hard and soft cornification in turtle epidermis. Micron 52–53, 8–15.
Alibardi, L., Thompson, M.B., 1999. Epidermal differentiation during carapace and plastron formation in the embryonic turtle Emydura macquarii. J. Anat. 194 (Pt 4), 531–545.
Alibardi, L., Thompson, M., 2006. Cytochemical, biochemical and molecular aspects of the process of keratinization in the epidermis of reptilian scales. Prog. Histochem. Cytochem. 40, 73–134.
Alibardi, L., Toni, M., 2006. Skin structure and cornification proteins in the soft-shelled turtle Trionyx spiniferus. Zoology 109 (3), 182–195.
Ashby, M.F., 1983. The mechanical properties of cellular solids. Metall. Trans. A. 14A, 1755–1769.
Ashman, R.B., Corin, J.D., Turner, C.H., 1987. Elastic properties of cancellous bone: measurement by an ultrasonic technique. J. Biomech. 20, 979–983.
Askari, E., Mehrali, M., Metselaar, I.H.S.C., Kadri, N.A., Rahman, M.M., 2012. Fabrication and mechanical properties of Al2O3/SiC/ZrO2 functionally graded material by electrophoretic deposition. J. Mech. Behav. Biomed. Mater. 12, 144–150.
Balani, K., Patel, R.R., Keshri, A.K., Lahiri, D., Agarwal, A., 2011. Multi-scale hierarchy of Chelydra serpentina: microstructure and mechanical properties of turtle shell. J. Mech. Behav. Biomed. Mater. 4, 1440–1451.
Barthelat, F., Espinosa, H.D., 2007. An experimental investigation of deformation and fracture of nacre–mother of pearl. Exp. Mech. 47 (3), 311–324.
Bar-On, B., Barth, F.G., Fratzl, P., Politi, Y., 2014. Multiscale structural gradients enhance the biomechanical functionality of the spider fang. Nat. Commun., 5.
Beniash, E., 2011. Biominerals—hierarchical nanocomposites: the example of bone. Wiley Interdiscip. Rev. Nanomed. Nanobiotechnol. 3 (1), 47–69.
Bitzer, T.N., 2012. Honeycomb Technology: Materials, Design, Manufacturing, Applications and Testing. Springer Science & Business Media.
Bogoslovov, R.B., Roland, C.M., Gamache, R.M., 2007. Impact-induced glass transition in elastomeric coatings. Appl. Phys. Lett. 90 (22), [221910-221910].
Bojanus, L. H., 1819. Anatome testudinis Europaeae (No. 26). Society for the Study of Amphibians and Reptiles.
Bonser, R., Purslow, P., 1995. The Young's modulus of feather keratin. J. Exp. Biol. 198 (4), 1029–1033.
Branch, W.R., Els, S.F., 1990. Predation on the angulate tortoise Chersina angulata by the kelp gull Larus dominicanus on Dassen Island. West. Cape. S. Afr. J. Zool. 25, 235–237.
Bruet, B.J., Song, J., Boyce, M.C., Ortiz, C., 2008. Materials design principles of ancient fish armour. Nat. Mater. 7 (9), 748–756.
Browning, A., Ortiz, C., Boyce, M.C., 2013. Mechanics of composite elasmoid fish scale assemblies and their bioinspired analogues. J. Mech. Behav. Biomed. Mater. 19, 75–86.
Byrne, D.P., Lacroix, D., Planell, J.A., Kelly, D.J., Prendergast, P.J., 2007. Simulation of tissue differentiation in a scaffold as a function of porosity, Young's modulus and dissolution rate: application of mechanobiological models in tissue engineering. Biomaterials 28 (36), 5544–5554.
Chen, I.H., Kiang, J.H., Correa, V., Lopez, M.I., Chen, P.-Y., McKittrick, J., et al., 2011. Armadillo armor: mechanical testing and micro-structural evaluation. J. Mech. Behav. Biomed. Mater. 4, 713–722.
Chimiak, W.J., 1996. U.S. Patent No. 5,514,017. Washington, DC: U.S. Patent and Trademark Office.
Chintapalli, R.K., Mirkhalaf, M., Dastjerdi, A.K., Barthelat, F., 2014. Fabrication, testing and modeling of a new flexible armor inspired from natural fish scales and osteoderms. Bioinspir. Biomim. 9 (3), 036005.
Christiansen, P., Wroe, S., 2007. Bite forces and evolutionary adaptations to feeding ecology in carnivores. Ecology 88 (2), 347–358.
Chundawat, T.S., Vaya, D., Sini, N.K., Varma, I.K., 2016. Blast mitigation using FRP retrofitting and coating techniques. Polym. Compos.. http://dx.doi.org/10.1002/pc.24116.
Collombet, F., Lalbin, X., Lataillade, J.L., 1998. Impact behavior of laminated composites: physical basis for finite element analysis. Compos. Sci. Technol. 58 (3), 463–478.
Congdon, J.D., Gibbons, J.W., 1990. Turtle eggs: their ecology and evolution. In: Gibbons, J.W. (Ed.), Life History and Ecolgy of the Slider Turtle. Smithsonian Press, Washington, D.C.
Currey, J.D., 2002. Bones: Structure and Mechanics.. Princeton University Press, Oxford.
Dalla Valle, L., Michieli, F., Benato, F., Skobo, T., Alibardi, L., 2013. Molecular characterization of alpha-keratins in comparison to associated beta-proteins in soft-shelled and hard-shelled turtles produced during the process of epidermal differentiation. J. Exp. Zool. Part B: Mol. Dev. Evol. 320, 428–441.
Damiens, R., Rhee, H., Hwang, Y., Park, S.J., Hammi, Y., Lim, H., Horstemeyer, M.F., 2012. Compressive behavior of a turtle's shell: experiment, modeling, and simulation. J. Mech. Behav. Biomed. Mater. 6, 106–112.
Ehrlich, H., 2015. Materials Design Principles of Fish Scales and ArmorBiological Materials of Marine Origin. Springer, Netherlands, 237–262.
Emmons, L.H., 1989. Jaguar predation on chelonians. J. Herpetol. 23, 311–314.
Erickson, G.M., Lappin, A.K., Vliet, K.A., 2003. The ontogeny of bite-force performance in American alligator (Alligator mississippiensis). J. Zool. Lond. 260, 317–327.
Faingold, A., Cohen, S.R., Wagner, H.D., 2012. Nanoindentation of osteonal bone lamellae. J. Mech. Behav. Biomed. 9, 198–206.
Farran, L., Ennos, A.R., Starkie, M., Eichhorn, S.J., 2009. Tensile and shear properties of fingernails as a function of a changing humidity environment. J. Biomech. 42 (9), 1230–1235.
Fish, J.F., Stayton, C.T., 2014. Morphological and mechanical changes in juvenile red-eared slider turtle (Trachemys scripta elegans) shells during ontogeny. J. Morphol. 275 (4), 391–397.
Fratzl, P., Gupta, H.S., Paschalis, E.P., Roschger, P., 2004. Structure and mechanical quality of the collagen–mineral nano-composite in bone. J. Mater. Chem. 14, 2115–2123.
Fudge, D.S., Gardner, K.H., Forsyth, V.T., Riekel, C., Gosline, J.M., 2003. The mechanical properties of hydrated intermediate filaments: insights from hagfish slime threads. Biophys. J. 85 (3), 2015–2027.
Gaunt, A.S., Gans, C., 1969. Mechanics of respiration in the snapping turtle, Chelydra serpentina (Linné). J. Morphol. 128 (2), 195–227.
Gibson, L.J., 2005. Biomechanics of cellular solids. J. Biomech. 38, 377–399.
Gilbert, S.F., Loredo, G.A., Brukman, A., Burke, A.C., 2001. Morphogenesis of the turtle shell: the development of a novel structure in tetrapod evolution. Evolut. Dev. 3, 47–58.
Goldstein, S.A., 1987. The mechanical properties of trabecular bone: dependence on anatomic location and function. J. Biomech. 20, 1055–1061.
Guidoni, G., Swain, M., Jager, I., 2009. Nanoindentation of wet and dry compact bone: influence of environment and indenter tip geometry on the indentation modulus. Philos. Mag. Lett. 90, 553–565.
Gupta, H.S., Zioupos, P., 2008. Fracture of bone tissue: the 'hows' and the 'whys'. Med. Eng. Phys. 30, 1209–1226.
Heithaus, M.R., Wirsing, A.J., Thomson, J.A., Burkholder, D.A., 2008. A review of lethal and non-lethal effects of predators on adult marine turtles. J. Exp. Mar. Biol. Ecol. 356, 43–51.
Hu, D.L., Sielert, K., Gordon, M., 2012. Turtle shell and mammal skull resistance to fracture due to predator bites and ground impact. J. Mech. Mater. Struct. 6 (9), 1197–1211.
Imbeni, V., Kruzic, J.J., Marshall, G.W., Marshall, S.J., Ritchie, R.O., 2005. The dentin–enamel junction and the fracture of human teeth. Nat. Mater. 4 (3), 229–232.
Iverson, J.B., 1991. Patterns of survivorship in turtles (order Testudines). Can. J. Zool. 69 (2), 385–391.
Jackson, D.C., 2002. Hibernating without oxygen: physiological adaptations of the painted turtle. J. Physiol. 543 (3), 731–737.
Jaslow, C.R., 1990. Mechanical properties of cranial sutures. J. Biomech. 23 (4),

313–321.
Kolednik, O., 2000. The yield stress gradient effect in inhomogeneous materials. Int. J. Solids Struct. 37 (5), 781–808.
Krauss, S., Monsonego-Ornan, E., Zelzer, E., Fratzl, P., Shahar, R., 2009. Mechanical function of a complex three-dimensional suture joining the bony elements in the shell of the red-eared slider turtle. Adv. Mater. 21, 407–412. http://dx.doi.org/10.1002/adma.200801256.
Launey, M.E., Chen, P.Y., McKittrick, J., Ritchie, R.O., 2009. Mechanistic aspects of the fracture toughness of elk antler bone. Acta Biomater. 6, 1505–1514.
Lawn, B.R., Cook, R.F., 2012. Probing material properties with sharp indenters: a retrospective. J. Mater. Sci. 42, 1–22.
Lazarev, Y.A., Grishkovsky, B.A., Khromova, T.B., Lazareva, A.V., 1985. Amide I band spectrum and structure of collagen and related polypeptides. Biopolymers 24, 1449–1478.
Lazarev, Y.A., Grishkovsky, B.A., Khromova, T.B., Lazareva, A.V., Grechishko, V.S., 1992. Bound water in the collagen-like triple-helical structure. Biopolymers 32, 189–195.
Li, Y., Ortiz, C., Boyce, M.C., 2011. Stiffness and strength of suture joints in nature. Phys. Rev. E. 84 (6), 062904.
Li, B.W., Zhao, H.P., Qin, Q.H., Feng, X.Q., Yu, S.W., 2012. Numerical study on the effects of hierarchical wavy interface morphology on fracture toughness. Comput. Mater. Sci. 57, 14–22.
Luschi, P., Åkesson, S., Broderick, A.C., Glen, F., Godley, B.J., Papi, F., Hays, G.C., 2001. Testing the navigational abilities of ocean migrants: displacement experiments on green sea turtles (Chelonia mydas). Behav. Ecol. Sociobiol. 50 (6), 528–534.
Lyson, T.R., Bever, G.S., Scheyer, T.M., Hsiang, A.Y., Gauthier, J.A., 2013. Evolutionary origin of the turtle shell. Curr. Biol. 23 (12), 1113–1119.
Lyson, T.R., Rubidge, B.S., Scheyer, T.M., de Queiroz, K., Schachner, E.R., Smith, R.M., et al., 2016. Fossorial origin of the turtle shell. Curr. Biol. 26 (14), 1887–1894.
Magwene, P.M., Socha, J.J., 2013. Biomechanics of turtle shells: how whole shells fail in compression. J. Exp. Zool. A. Ecol. Genet. Physiol. 319, 86–98.
Mao, H., Wagner, C., Guan, F., Yeni, Y.N., Yang, K.H., 2011. Material properties of adult rat skull. J. Mech. Med. Biol. 11 (05), 1199–1212.
McKittrick, J., Chen, P.-Y., Bodde, S.G., Yang, W., Novitskaya, E.E., Meyers, M.A., 2012. The structure, functions, and mechanical properties of keratin. JOM-J. Min. Met. Mat. S. 64, 449–467.
Motherway, J.A., Verschueren, P., Van der Perre, G., Vander Sloten, J., Gilchrist, M.D., 2009. The mechanical properties of cranial bone: the effect of loading rate and cranial sampling position. J. Biomech. 42 (13), 2129–2135.
Moita, J.S., Araújo, A.L., Soares, C.M., Soares, C.M., 2013. Finite element model for damping optimization of viscoelastic sandwich structures. Adv. Eng. Softw. 66, 34–39.
Naleway, S.E., Taylor, J.R., Porter, M.M., Meyers, M.A., McKittrick, J., 2016. Structure and mechanical properties of selected protective systems in marine organisms. Mater. Sci. Eng. C. 59, 1143–1167.
Pailler-Mattei, C., Bec, S., Zahouani, H., 2008. In vivo measurements of the elastic mechanical properties of human skin by indentation tests. Med. Eng. Phys. 30 (5), 599–606.
Peterlik, H., Roschger, P., Klaushofer, K., Fratzl, P., 2006. From brittle to ductile fracture of bone. Nat. Mater. 5, 52–55.
Petras, A., Sutcliffe, M.P.F., 1999. Failure mode maps for honeycomb sandwich panels. Compos. Struct. 44 (4), 237–252.
Polly, P.D., Stayton, C.T., Dumont, E.R., Pierce, S.E., Rayfield, E.J., Angielczyk, K.D., 2016. Combining geometric morphometrics and finite element analysis with evolutionary modeling: towards a synthesis. J. Vertebr. Paleontol.. http://dx.doi.org/10.1080/02724634.2016.1111225.
Raabe, D., Sachs, C., Romano, P., 2005. The crustacean exoskeleton as an example of a structurally and mechanically graded biological nanocomposite material. Acta Mater. 53, 4281–4292.
Rafferty, K.L., Herring, S.W., 1999. Craniofacial sutures: morphology, growth, and in vivo masticatory strains. J. Morphol. 242 (2), 167.
Raman, S.N., Ngo, T., Mendis, P., Pham, T., 2012. Elastomeric polymers for retrofitting of reinforced concrete structures against the explosive effects of blast. Adv. Mater. Sci. Eng.. http://dx.doi.org/10.1155/2012/754142.
Rhee, H., Horstemeyer, M.F., Hwang, Y., Lim, H., El Kadiri, H., Trim, W., 2009. A study on the structure and mechanical behavior of the Terrapene Carolina carapace: a pathway to design bio-inspired synthetic composites. Mater. Sci. Eng. C. Mater. Biol. Appl. 29, 2333–2339.
Rhee, H., Horstemeyer, M.F., Ramsay, A., 2011. A study on the structure and mechanical behavior of the Dasypus novemcinctus shell. Mater. Sci. Eng. C. Mater. Biol. Appl. 31, 363–369.
Rho, J.Y., Currey, J.D., Zioupos, P., Pharr, G.M., 2001a. The anisotropic Young's modulus of equine secondary osteons and interstitial bone determined by nanoindentation. J. Exp. Biol. 204, 1775–1781.
Rho, J.Y., Mishra, S.R., Chung, K., Bai, J., Pharr, G.M., 2001b. Relationship between ultrastructure and the nanoindentation properties of intramuscular herring bones. Ann. Biomed. Eng. 29, 1082–1088.
Rivera, G., Stayton, C.T., 2011. Finite element modeling of shell shape in the freshwater turtle Pseudemys concinna reveals a trade-off between mechanical strength and hydrodynamic efficiency. J. Morphol. 272 (10), 1192–1203.
Roland, C.M., Fragiadakis, D., Gamache, R.M., 2010. Elastomer–steel laminate armor. Compos. Struct. 92, 1059–1064.
Samiee, A., Amirkhizi, A.V., Nemat-Nasser, S., 2013. Numerical study of the effect of polyurea on the performance of steel plates under blast loads. Mech. Mater. 64, 1–10.
Scheyer, T.M., Sánchez-Villagra, M.R., 2007. Carapace bone histology in the giant pleurodiran turtle Stupendemys geographicus: phylogeny and function. Acta. Palaeontol. Pol. 52, 1.
Scheyer, T.M., Danilov, I.G., Sukhanov, V.B., Syromyatnikova, E.V., 2014. The shell bone histology of fossil and extant marine turtles revisited. Biol. J. Linn. Soc. 112 (4), 701–718.
Scheyer, T.M., Pérez-García, A., Murelaga, X., 2015. Shell bone histology of solemydid turtles (stem Testudines): palaeoecological implications. Org. Divers. Evol. 15 (1), 199–212.
Schulz, U., Peters, M., Bach, F.W., Tegeder, G., 2003. Graded coatings for thermal, wear and corrosion barriers. Mat. Sci. Eng. A. 362 (1), 61–80.
Shen, H.S., 2016. Functionally graded materials: nonlinear analysis of plates and shells.. CRC press.
Shelef, Y., Bar-On, B., 2017. Surface protection in bio-shields via a functional soft skin layer: lessons from the turtle shell. J. Mech. Behav. Biomed..
Simha, N.K., Fischer, F.D., Koledni, O., Chen, C.R., 2003. Inhomogeneity effects on the crack driving force in elastic and elastic–plastic materials. J. Mech. Phys. Solids 51 (1), 209–240.
Sola, A., Bellucci, D., Cannillo, V., 2016. Functionally graded materials for orthopedic applications–an update on design and manufacturing. Biotechnol. Adv.. http://dx.doi.org/10.1016/j.biotechadv.2015.12.013.
Soons, J., Herrel, A., Genbrugge, A., Adriaens, D., Aerts, P., Dirckx, J., 2012. Multi-layered bird beaks: a finite-element approach towards the role of keratin in stress dissipation. J. R. Soc. Interface 9 (73), 1787–1796.
Stayton, C.T., 2009. Application of thin-plate spline transformations to finite element models, or, how to turn a bog turtle into a spotted turtle to analyze both. Evolution 63, 1348–1355.
Stayton, C.T., 2011. Biomechanics on the half shell: functional performance influences patterns of morphological variation in the emydid turtle carapace. Zoology 114 (4), 213–223.
Sun, C.Y., Chen, P.Y., 2013. Structural design and mechanical behavior of alligator (Alligator mississippiensis) osteoderms. Acta Biomater. 9 (11), 9049–9064.
Tasdemirci, A., Tunusoglu, G., Güden, M., 2012. The effect of the interlayer on the ballistic performance of ceramic/composite armors: experimental and numerical study. Int. J. Impact Eng. 44, 1–9.
Taylor, A.M., Bonser, R.H.C., Farrent, J.W., 2004. The influence of hydration on the tensile and compressive properties of avian keratinous tissues. J. Mater. Sci. 39 (3), 939–942.
Tekalura, S.A., Shukla, A., Shivakumar, K., 2008. Blast resistance of polyurea based layered composite materials. Compos. Struct. 84, 271–281.
Thieme, M., Wieters, K.P., Bergner, F., Scharnweber, D., Worch, H., Ndop, Kim, T.J., Grill, W., 2001. Titanium powder sintering for preparation of a porous functionally graded material destined for orthopaedic implants. . J. Mater. Sci. Mater. Med. 12 (3), 225–231.
Torres, F.G., Malásquez, M., Troncoso, O.P., 2015. Impact and fracture analysis of fish scales from Arapaima gigas. Mater. Sci. Eng. C. 51, 153–157.
Vega, C., Stayton, C.T., 2011. Dimorphism in shell shape and strength in two species of emydid turtle. Herpetologica 67 (4), 397–405.
Vernerey, F.J., Barthelat, F., 2010. On the mechanics of fishscale structures. Int. J. Solids Struct. 47, 2268–2275.
Walley, H.D., 1993. Chelydra serpentina (Snapping Turtle). Predation. Herpetol. Rev. 24, 148–149.
Wang, B., Yang, W., McKittrick, J., Meyers, M.A., 2016. Keratin: structure, mechanical properties, occurrence in biological organisms, and efforts at bioinspiration. Prog. Mater. Sci. 76, 229–318.
Wei, G., Bhushan, B., Torgerson, P.M., 2005. Nanomechanical characterization of human hair using nanoindentation and SEM. Ultramicroscopy 105 (1), 248–266.
Weiner, S., Wagner, H.D., 1998. The material bone: structure-mechanical function relations. Annu. Rev. Mater. Sci. 28, 271–298.
Yadav, S., Ravichandran, G., 2003. Penetration resistance of laminated ceramic/polymer structures. Int. J. Impact Eng. 28 (5), 557–574.
Yang, L., 2015. Particle Dynamics Simulation of Microstructure Evolution towards Functionally Graded Material Manufacturing [Ph.D Dissertation]. Columbia University.
Yang, W., Chen, I.H., Gludovatz, B., Zimmermann, E.A., Ritchie, R.O., Meyers, M.A., 2013. Natural flexible dermal armor. Adv. Mater. 25 (1), 31–48.
Yu, W., Zhu, K., Aman, Y., Guo, Z., Xiong, S., 2016. Bio-inspired design of SiC f-reinforced multi-layered Ti-intermetallic composite. Mater. Des. 101, 102–108.
Zhu, D., Ortega, C.F., Motamedi, R., Szewciw, L., Vernerey, F., Barthelat, F., 2012. Structure and mechanical performance of a modern fish scale. Adv. Eng. Mater. 14, B185–B194.
Zhu, D., Szewciw, L., Vernerey, F., Barthelat, F., 2013. Puncture resistance of the scaled skin from striped bass: collective mechanisms and inspiration for new flexible armor designs. J. Mech. Behav. Biomed. Mater. 24, 30–40.
Zhu, K., Yu, W., Aman, Y., Jing, T., 2016. Synthesis, microstructure and mechanical properties of a bio-inspired Ti-intermetallic multi-layered/SiCf. J. Mater. Sci. 51 (18), 8747–8760.
Zimmermann, E.A., Gludovatz, B., Schaible, E., Dave, N.K., Yang, W., Meyers, M.A., Ritchie, R.O., 2013. Mechanical adaptability of the Bouligand-type structure in natural dermal armour. Nat. Commun., 4.